USE OF SPLINE INTERPOLATION FOR BORDER DEFINITION FROM TWO-DIMENSIONAL ECHOCARDIOGRAMS: COMPARISON TO MANUAL METHOD

by

Antoinette Fay Ryser

A thesis submitted to the faculty of
The University of Utah
in partial fulfillment of the requirements for the degree of

Master of Science

Department of Medical Biophysics and Computing

The University of Utah

June 1985

THE UNIVERSITY OF UTAH GRADUATE SCHOOL

SUPERVISORY COMMITTEE APPROVAL

of a thesis submitted by

Antoinette Fay Ryser

This thesis has been read by each member of the following supervisory committee and by majority vote has been found to be satisfactory.

5/30/85

Dennis L. Parker

Arthur D. Hagan

THE UNIVERSITY OF UTAH GRADUATE SCHOOL

FINAL READING APPROVAL

To the Graduate Council of The University of Utah:

I have read the thesis of Antoinette Fay Ryser in its final form and have found that (1) its format, citations, and bibliographic style are consistent and acceptable; (2) its illustrative materials including figures, tables, and charts are in place; and (3) the final manuscript is satisfactory to the Supervisory Committee and is ready for submission to the Graduate School.

Date

Member, Supervisory Committee

Approved for the Major Department

Homer R. Warner
Chairman, Dean

Approved for the Graduate Council

ABSTRACT

A semiautomatic method for definition of cardiac chamber borders from two-dimensional echocardiograms has been developed which incorporates spline interpolation to produce a smooth curve with moderate operator involvement. This research compares the semiautomatic border definition (SBD) method to the currently used manual border definition (MBD) method according to the following criteria: time requirements, storage requirements, reproducibility, and accuracy.

A paired t-test showed the mean contour generation time over multiple observers, patients, trials and cardiac contours to be significantly greater for SBD than for MBD (p=0). The mean number of stored border points for SBD was 9 ± 3.84. Manual contours each required 64 stored border points to maintain contour integrity. Reproducibility of 6 cardiac contours was compared via a sign test analysis of variances of 64 radial or hemichordal lengths recorded from contours generated over multiple observers, trials and patients. SBD produced significantly more reproducible contours for the short axis view at the mitral valve level at end-diastole (p=0) and at end-systole (p=0) and for the apical four-chamber view at end-diastole (p=0). There was no significant difference in reproducibility between methods for the apical four-chamber view at end-systole (p=.136) and the apical two-chamber view at end-diastole (p=.784). Only the apical two-chamber view at end-systole proved to be significantly more reproducible using MBD (p=.046). Accuracy of methods was compared by generating contours from black-on-

white phantom images for which the true border coordinates were known. A mean absolute radial difference was calculated from 64 radial measurements taken from each contour and a paired t-test comparing these values between methods showed SBD to be significantly more accurate than MBD ($p=0$).

Time requirements for SBD are highly machine dependent and may be significantly reduced with upgraded hardware. Subjectively, SBD appears to be less tedious and less fatiguing for the operator. For these reasons and because it has been shown to produce more accurate and equally reproducible or more reproducible contours than MBD, SBD appears to be the preferred method for two-dimensional echocardiographic contour generation.

TABLE OF CONTENTS

LIST OF TABLES

LIST OF FIGURES

ACKNOWLEDGEMENTS

Special thanks to T. Allen Pryor for assistance, friendship, and support for the duration of this research project, and to Dennis L. Parker for his suggestions and enthusiasm. Also thanks to the Department of Medical Biophysics and Computing, University of Utah, for my research fellowship.

I.

INTRODUCTION

Off-line computerized analysis of two-dimensional echocardiograms has been shown to produce clinically meaningful quantitative measures of several cardiac parameters(1-3). Chamber volumes and ejection fractions may be calculated using area and linear measurements from several cardiac planes. These parameters are relevant in the evaluation of cardiac function. Regional wall motion and thickening indices are determined by using segmental areas, chordal lengths, or radial lengths. These indices play a potentially significant role in the identification and categorization of left ventricular myocardial infarction sites(1).

In order to obtain area or radial measurements the cardiac chamber border must be defined. Several border definition algorithms, incorporating various degrees of operator involvement, have been devised for this purpose.

Automatic border definition systems generally process two-dimensional echocardiographic images to present a more identifiable border via spatial and temporal averaging or integration of pixel intensities, frequently in conjunction with dynamic grey-level range expansion(4-6). Borders are identified through grey-level thresholding or convolution techniques(4,5). Clinical use of these techniques is presently severely

limited by their inability to recognize imaging artifacts, non-wall cardiac structures, and areas of echo drop-out, necessitating operator correction which takes time and reintroduces the subjectivity that automated border definition proposes to alleviate.

Most computerized cardiac contouring systems in clinical use today utilize magnetic bitpad or light pen systems which oblige the technician or echocardiographer to trace the cardiac chamber borders manually. Manual tracing allows good definition of chamber borders, but is slow and tedious, requires a relatively large amount of computer memory to store border coordinates, and is subject to drawing inaccuracies that may affect radial or segmental area measurements.

Studies have shown that most of the present border definition systems allow accurate and reproducible measurement of chamber areas and volumes, with only an insignificant amount of variability(7,8). However, errors and/or variability in border definition have a more dramatic effect on measurements of segmental areas, chordal lengths, and radial lengths because the percent of error at a given point of the border is much greater for segmental area or length measurements than for the total area of the contour. Neither automatic nor manual border definition systems have proven totally adequate for regional wall motion and thickening studies which incorporate these measurements. Automatic systems are currently impractical because they require manual correction and they do not generally offer significantly greater reproducibility than other less complex methods. Manual border definition (MBD) tends to introduce high frequency noise into the contour which may affect the resulting measurements. This dilemma has provided the impetus

for the current effort to develop a timely, convenient technique for border definition that minimizes point variability and maximizes reproducibility.

A semiautomatic border definition (SBD) system has been developed which permits an echocardiographer or technician to identify several representative border points (RBPs) between which the computer generates a smooth curve using linear interpolation. The operator can add or change points until he judges the resulting contour to be acceptable. This approach has the following possible advantages over the previously described border definition systems:

1. Contour generation is less tedious and may be less time consuming than current methods.
2. Contour storage requirements are considerably reduced since only a few operator-defined points need to be stored. For manual and automatic border definition systems a large number of points must be stored to maintain the integrity of the contour.
3. Drawing error may be reduced from that of MBD systems since only a few points need be entered rather than all border points, and high frequency noise is eliminated.

The SBD system developed for this research accomplishes linear interpolation through the use of the cubic spline function. The cubic spline appears to be the method of choice for this application since it generates a smooth curve free of high frequency noise that interpolates to all data points and is relatively easy to compute.

The purpose of this thesis is to compare the clinically current MBD method to the new SBD method according to the following criteria:

1. Time required to generate an acceptable contour.

2. Number of cartesian coordinate pairs necessary for storage of contours.
3. Accuracy of contours made from computer-generated images for which the true border coordinates are known.
4. Reproducibility of contours over multiple trials and observers.

II.

METHODS

Derivation of the Cubic Spline

Given an arbitrary number of data points which are represented as cartesian coordinates and are in ascending order with respect to the x-axis (Figure 1a), a curve may be interpolated through said data points using a spline function of any degree. The spline function S(x) consists of a series of polynomials which are unique on each subinterval, and are piecewise continuous. The formal definition of the spline function is as follows:

Let the interval I = a,b be divided into n-1 subintervals $a = a_1 < a_2 \ldots < a_{n-1} < a_n = b$ not necessarily equidistant. A spline S(x) of degree m is a function defined on I which:

1. Coincides with a polynomial of degree m on each subinterval $I_i = [a_{i-1},a_i]$ $i = 2,\ldots,n$.
2. Has continuous derivatives up to order m-1 where a_i $i = 1,\ldots,n$ are called the nodes or knots of the spline and represent the x-projections of the data points(9). In this presentation the nodes will have coordinates (a_i,y_i) where $S(a_i) = y_i$ $i = 1,\ldots,n$ for n data points.

The simplest spline consists of first order polynomials and this corresponds to straight line interpolation between data points as

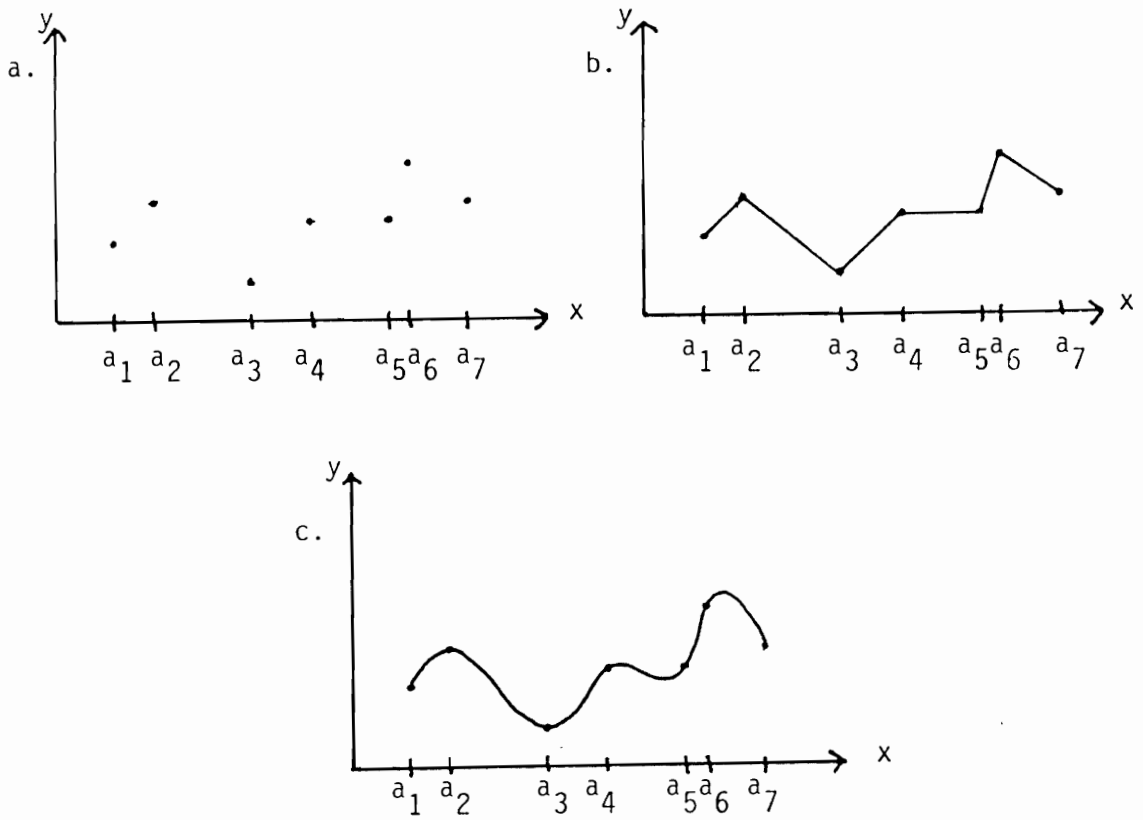

Figure 1. Spline Interpolation through arbitrary data points

a. Arbitrary number of data points, $\{a_i, y_i\}$ in ascending order with respect to the i^{th} x axis.
b. First order spline interpolation through all data points.
c. Third order spline interpolation through all data points.

illustrated in Figure 1b. A first order spline becomes smoother as the subintervals become very small, but both first and second order splines are subject to irregularities and sudden changes of slope at the nodes since neither has a second derivative. The third order or cubic spline has two continuous derivatives and thus can be constrained such that the changes of slope of adjoining pieced polynomials are equal at their common node, thus producing a smooth continuous curve without nodal irregularities (Figure 1c). A single high-order polynomial could also generally be found to fit all the data points, but it would most likely produce a curve rendered deficient of useful information by the violent oscillations attendant with its high order. The cubic spline alleviates this dilemma by employing polynomials of the smallest degree necessary to assure the continuity of the resulting function. Thus the cubic spline is a function of maximal smoothness(9).

The cubic spline algorithm used in the present research is derived as follows:

Since S(x) is a piecewise cubic function, its first derivative S'(x) must be piecewise quadratic and its second derivative S"(x) must be piecewise linear and piecewise continuous (Figure 2). It follows that the general equation of the second derivative on any subinterval I_i can be represented by the two-point equation of a line. From the general equation

$$y - y_1 = \frac{y_2 - y_1}{x_2 - x_1} (x - x_1)$$

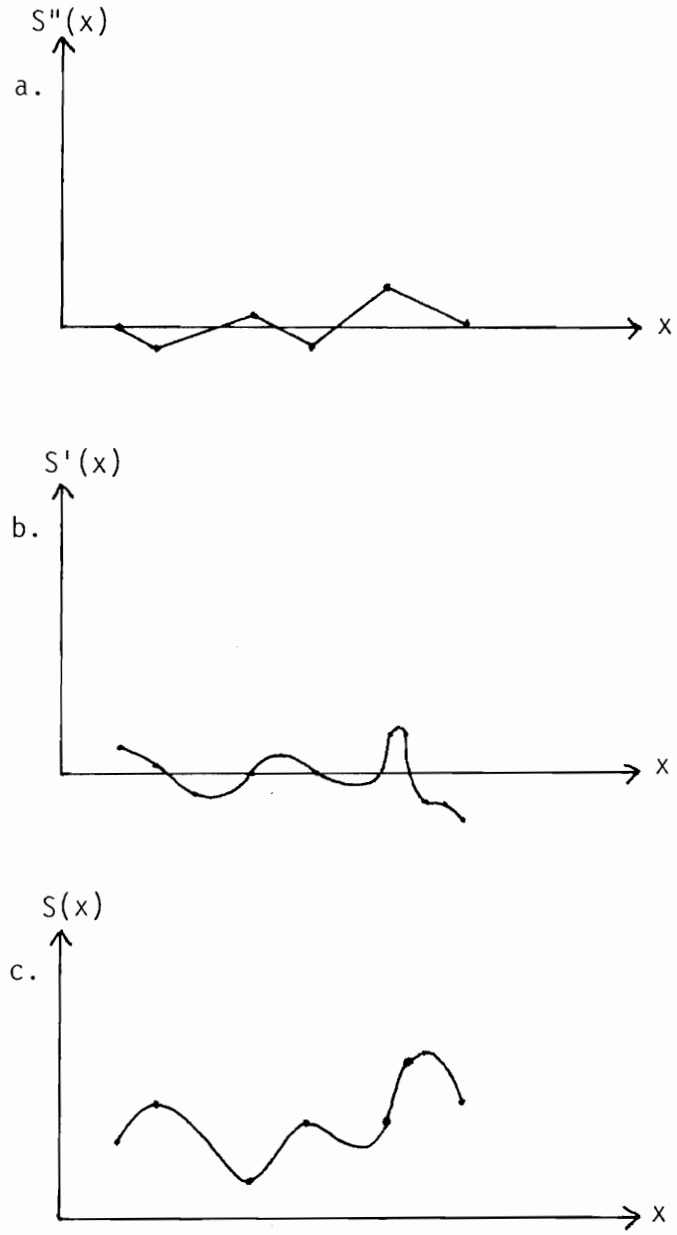

Figure 2. Derivatives of the cubic spline function

a. The second derivative of the cubic spline function shown in Figure 1c. The resulting function S"(x) is piecewise linear and piecewise continuous.
b. The first derivative of the cubic spline function shown in Figure 1c. The resulting function S'(x) is piecewise quadratic and piecewise continuous.
c. The cubic spline through all data points is piecewise cubic and continuous.

substitution of the points $(a_i, S''(a_i))$ and $(a_{i-1}, S''(a_{i-1}))$ yields

$$S''(x) - S''(a_{i-1}) = \frac{S''(a_i) - S''(a_{i-1})}{a_i - a_{i-1}} (x - a_{i-1})$$

Setting $M_i = S''(a_i)$ for $i = 1,\ldots,n$ and adding M_{i-1} to both sides gives

$$S''(x) = \frac{M_i - M_{i-1}}{a_i - a_{i-1}} (x - a_{i-1}) + M_{i-1}$$

which reduces algebraically to

$$S''(x) = M_{i-1} \frac{(a_i - x)}{a_i - a_{i-1}} + M_i \frac{(x - a_{i-1})}{a_i - a_{i-1}}$$

Setting $h_i = a_i - a_{i-1}$ for $i = 2,\ldots,n$, which is the length of one subinterval, yields

$$S''(x) = M_{i-1} \frac{(a_i - x)}{h_i} + M_i \frac{(x - a_{i-1})}{h_i}$$

It follows that $S(x)$ can be obtained by two simple integrations of eq.(1):

$$S'(x) = \int S''(x)dx = -M_{i-1} \frac{(a_i - x)^2}{2h_i} + M_i \frac{(x - a_{i-1})^2}{2h_i} + c_i$$

and continuing

$$S(x) = \int S'(x)dx = M_{i-1} \frac{(a_i - x)^3}{6h_i} + M_i \frac{(x - a_{i-1})^3}{6h_i} + c_i x + d_i$$

where c_i and d_i are integration constants.

$$\begin{aligned} \text{Setting } c_i x + d_i &= C_i(a_i - x) + D_i(x - a_{i-1}) \\ &= (D_i - C_i)x + C_i a_i - D_i a_{i-1} \\ &= C_i(a_i - x) + D_i(x - a_{i-1}) \end{aligned}$$

yields

$$S(x) = M_{i-1}\frac{(a_i - x)^3}{6h_i} + M_i\frac{(x - a_{i-1})^3}{6h_i} + C_i(a_i - x) + D_i(x - a_{i-1}) \tag{2}$$

which allows derivation of C_i and D_i by substituting the known values for x and S(x) (i.e.,$(a_i,S(a_i))$ and $(a_{i-1},S(a_{i-1}))$) at the nodes a_i and a_{i-1} into eq.(2). Letting $y_i = S(a_i)$ for i = 1,...,n results in the following equations for C_i and D_i:

$$C_i = \frac{(y_{i-1} - \frac{M_{i-1}h_i^2}{6})}{h_i} \tag{3}$$

and

$$D_i = \frac{(y_i - \frac{M_i h_i^2}{6})}{h_i} \tag{4}$$

Thus substituting eqs. (3) and (4) into eq.(2) yields the general formula for the cubic spline:

$$S(x) = M_{i-1}\frac{(a_i - x)^3}{6h_i} + M_i\frac{(x - a_{i-1})^3}{6h_i} + (y_{i-1} - \frac{M_{i-1}h_i^2}{6})\frac{(a_i - x)}{h_i}$$

$$+ (y_i - \frac{M_i h_i^2}{6})\frac{(x - a_{i-1})}{h_i} \qquad (5)$$

The above equation will produce a unique polynomial for each subinterval I_i where a_i is the x-projection of any data point and y_i is the y-projection of that point. The only remaining stumbling block in the calculation involves the determination of the value of M_i for $i = 1,\ldots,n$. This is done as follows:

Since it is known that at the nodes of the cubic spline function the slope $S'(a_i)$ must have the same value when approached from either side (Figure 2b), calculation of $S'(a_i-)$ and $S'(a_i+)$ will yield two unique equations for $S'(a)$ that must be equal. First taking the derivative of eq.(5) gives

$$S'(x) = -M_{i-1}\frac{(a_i - x)^2}{2h_i} + \frac{M_i(x - a_{i-1})^2}{2h_i} + \frac{y_i - y_{i-1}}{h_i} - \frac{M_i - M_{i-1}}{6}h_i$$

Then setting $x = a_i$ for the subinterval $I_i = [a_{i-1}, a_i]$ produces

$$S'(a_i-) = \frac{h_i}{6}M_{i-1} + \frac{h_i}{3}M_i + \frac{y_i - y_{i-1}}{h_i} \qquad (6)$$

and setting $x = a_i$ for the subinterval $I_{i+1} = [a_i, a_{i+1}]$ produces

$$S'(a_i+) = -\frac{h_{i+1}}{3}M_i - \frac{h_{i+1}}{6}M_{i+1} + \frac{y_{i+1} - y_i}{h_{i+1}} \qquad (7)$$

Equating eqs.(6) and (7) over the interval I results in n - 2 linear equations of the following form:

$$\frac{h_i}{6} M_{i-1} + \frac{h_i + h_{i+1}}{3} M_i + \frac{h_{i+1}}{6} M_{i+1} = \frac{y_{i+1} - y_i}{h_{i+1}} - \frac{y_i - y_{i-1}}{h_i}$$

$$\text{for } i = 2,\ldots,n \tag{8}$$

In the present application of the algorithm, all constants are abbreviated for ease of manipulation as follows:

$$\sigma_i = \frac{y_i - y_{i-1}}{h_i} \quad \text{for } i = 2,\ldots,n$$

$$\lambda_i = \frac{h_{i+1}}{h_i + h_{i+1}} \qquad \mu_i = 1 - \lambda_i \qquad d_i = \frac{6\,(\sigma_{i+1} - \sigma_i)}{h_i + h_{i+1}} \tag{9}$$

$$\text{for } i = 2,\ldots,n-1$$

When eq.(8) is algebraically rearranged to

$$\frac{h_i}{h_i + h_{i+1}} M_{i-1} + 2M_i + \frac{h_{i+1}}{h_i + h_{i+1}} M_{i+1} =$$

$$\frac{6}{h_i + h_{i+1}} \left[\frac{(y_{i+1} - y_i)}{h_{i+1}} - \frac{y_i - y_{i-1})}{h_i}\right]$$

substitution of the abbreviations of eqs.(9) can be made to yield a tridiagonal system of simultaneous linear equations of the form in

Figure 3, which can be easily solved using simple Gaussian Elimination without pivoting in a total of 3(n-1) additions and multiplications and (2n-1) divisions(10). It should be noted that the first and last rows of the matrix in Figure 3 represent two additional conditions derived from the assumption that $S''(x) = 0$ for all $x < a$ or $x > b$. Therefore $M_0 = M_{n+1} = 0$ (10).

The cubic spline function that has been described up to this point has diverse applications and for the purposes of this presentation it will be identified as the standard cubic spline. The remaining conditions necessary for the implementation of this algorithm are more application-specific and will be discussed in the following section.

Application of the Cubic Spline to Two-dimensional Echocardiogram Border Definition

In the present application experienced echocardiographers and echocardiographic technicians are attempting to identify and define via single point indicators the epicardial and endocardial boundaries of the heart chambers, most prominently of the left ventricle, from stop-frames of real-time videotaped two-dimensional echocardiograms. Figure 4 shows three left-ventricular cross-sections from a two-dimensional echocardiogram which demonstrate the general shapes and configurations of points through which a continuous contour must be generated. Note that the smooth curve approximating algorithm must be able to produce a closed curve (Figures 4a and 4b) with no irregularities at the starting/ending point, and must be easily modified to produce an open curve (Figures 4c,4d,4e, and 4f). The curve must be generated through a set of points which have a circular or banana-shaped orientation and are

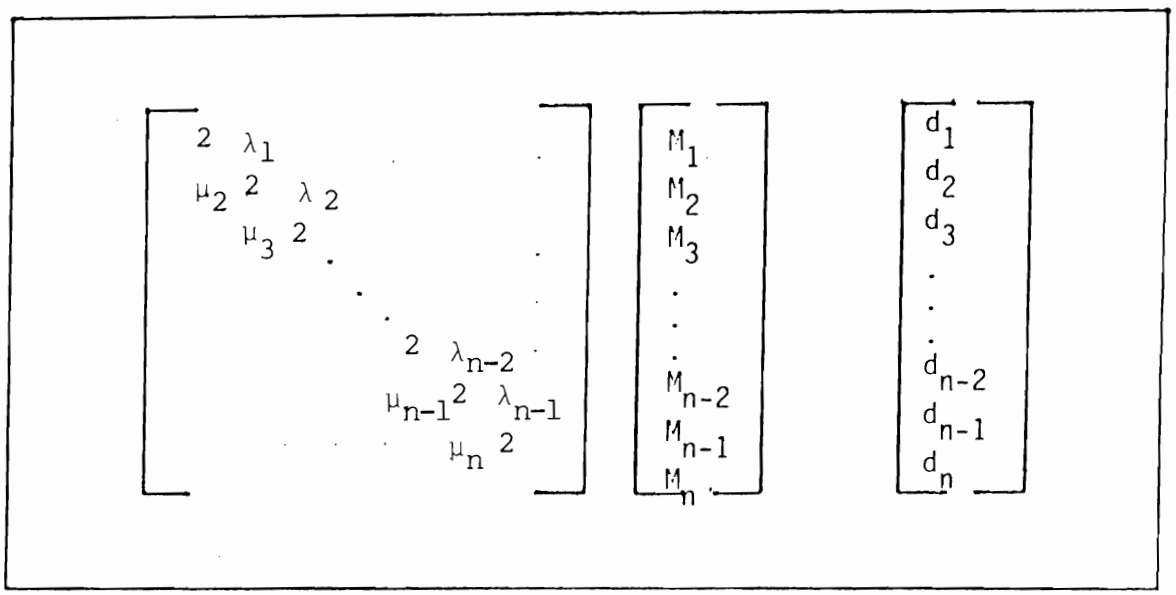

Figure 3. Tridiagonal matrix of simultaneous linear equations whose solution M_i $i = 1,\ldots,n$ represents the second derivative of the spline function $S(x)$ at the nodes $\{a_i, y_i\}$ $i = 1,\ldots,n$, where the constants λ_i, μ_i and d_i are determined from eqs. (9).

Figure 4. Three left ventricular cross-sections from a two-dimensional echocardiogram.

a. Two-dimensional echocardiographic short-axis view demonstrating appropriate placement of representative border points.
b. Parametric spline function interpolated through the points in (a).
c. Two-dimensional echocardiographic apical four-chamber view demonstrating appropriate placement of representative border points.
d. Parametric spline function interpolated through the points in (c).
e. Two-dimensional echocardiographic apical two-chamber view demonstrating appropriate placement of representative border points.
f. Parametric spline function generated through the points in (e).

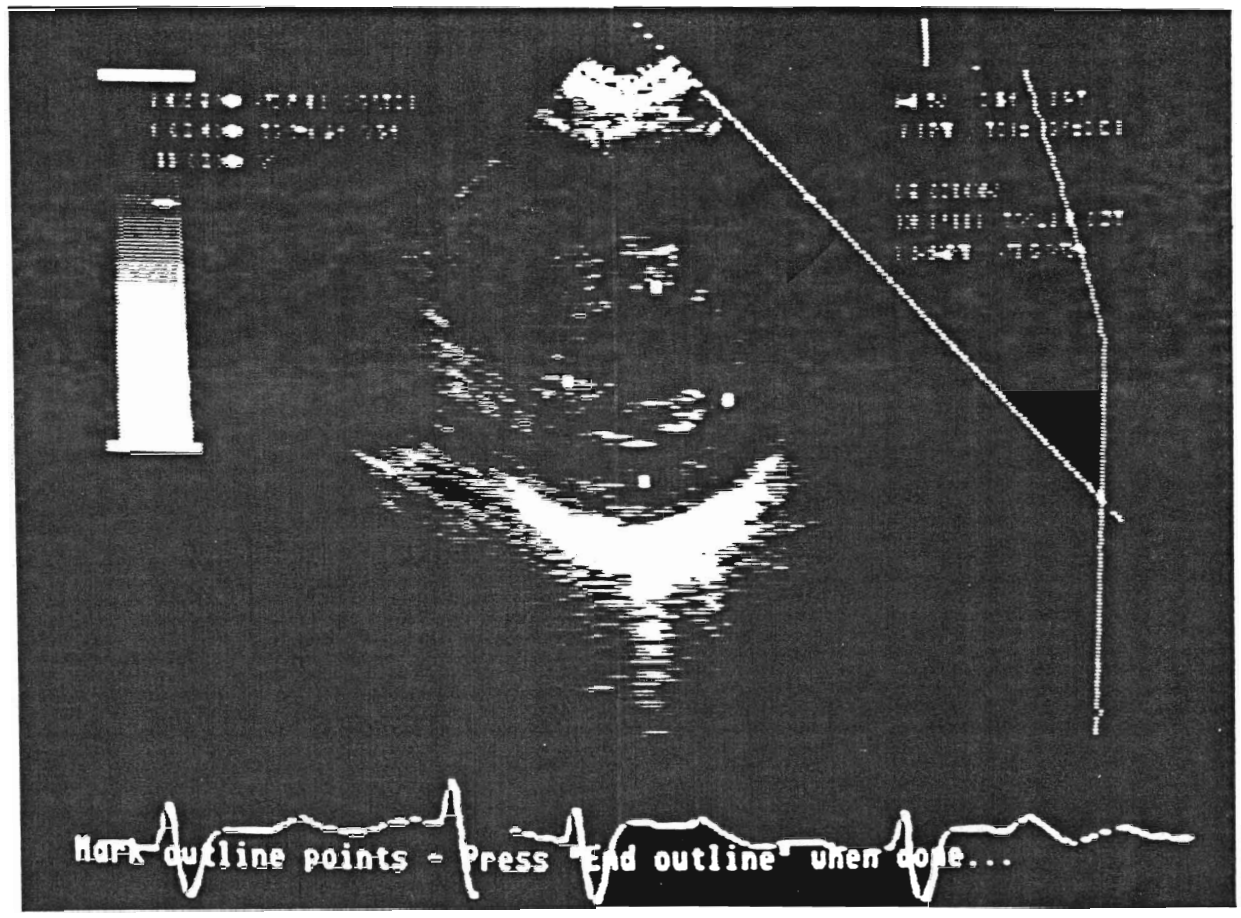

Figure 4a.

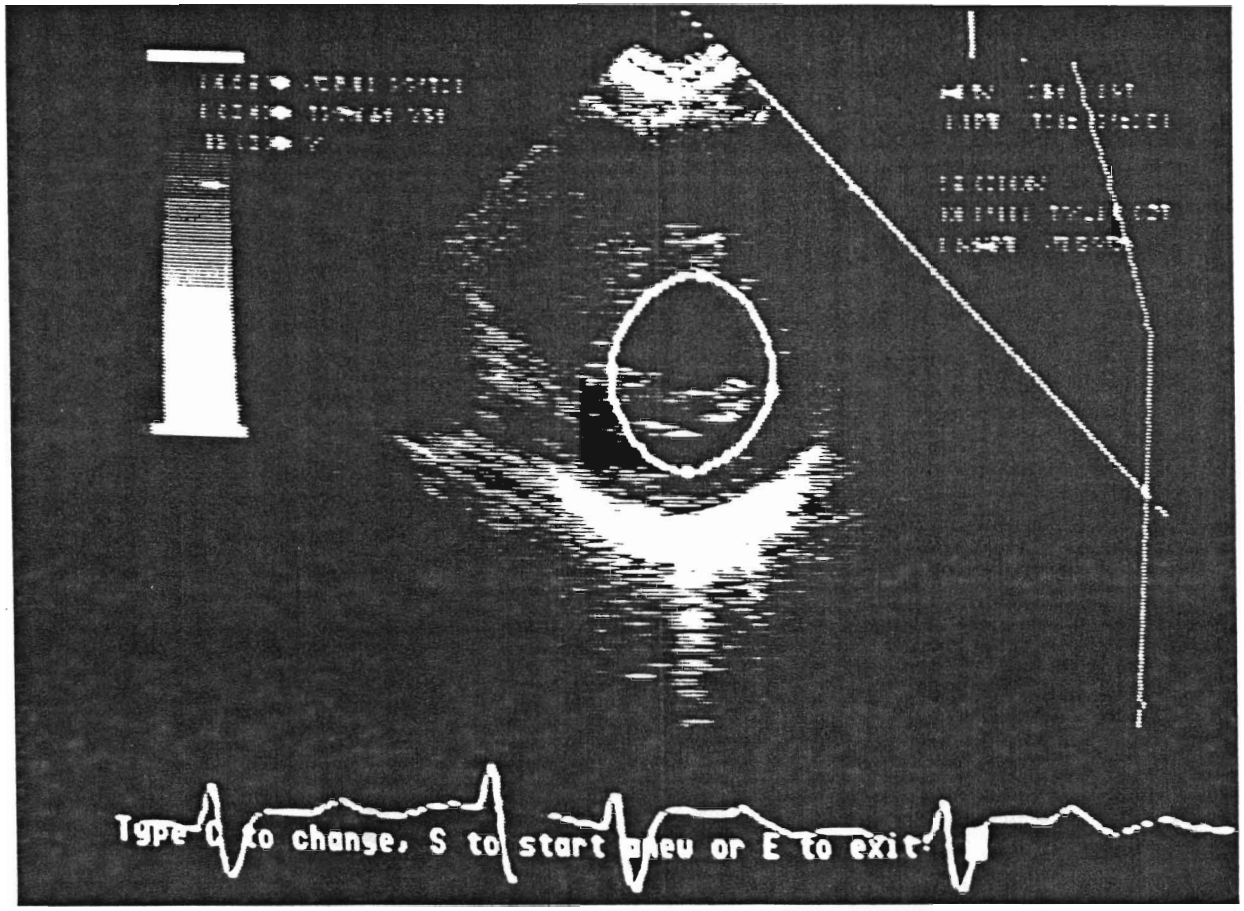

Figure 4b.

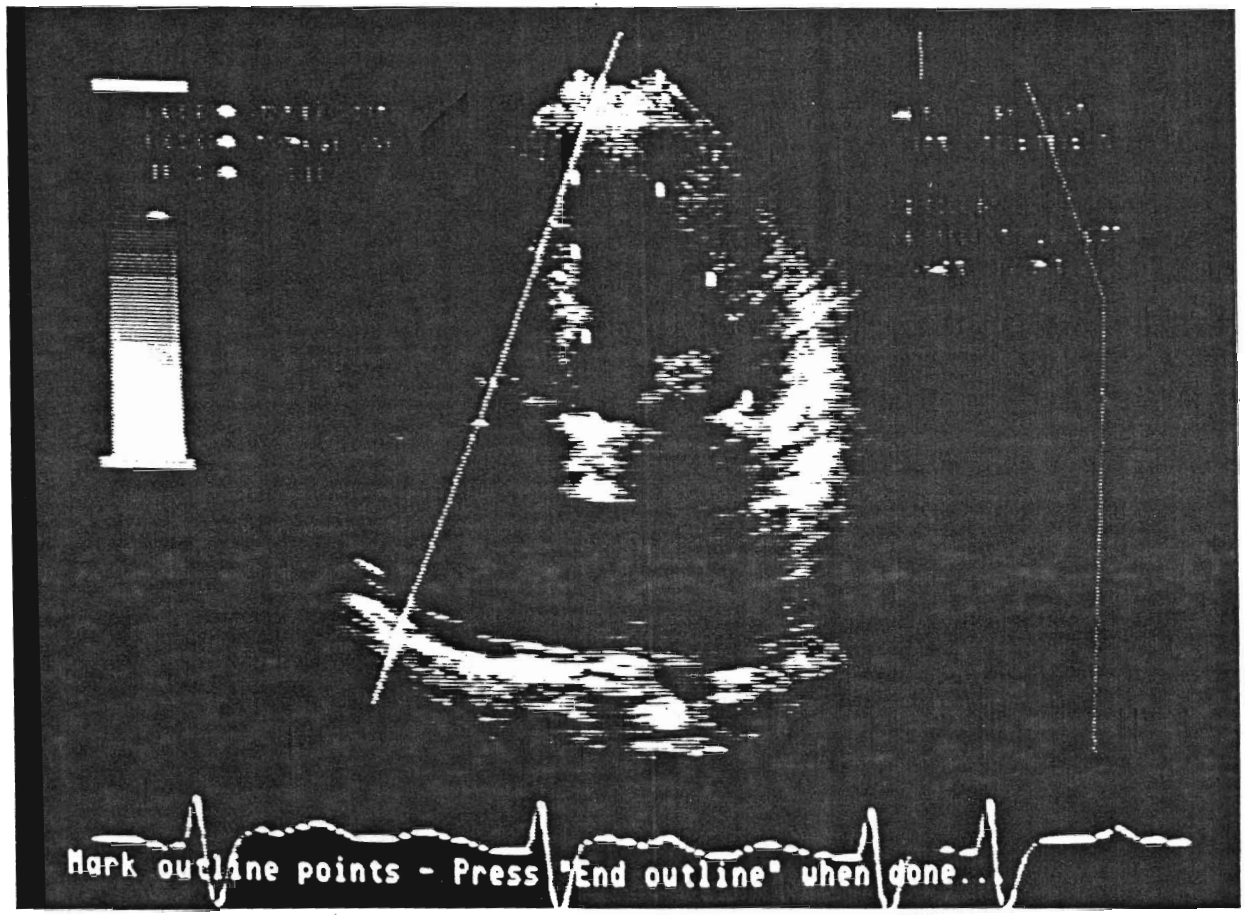

Figure 4c.

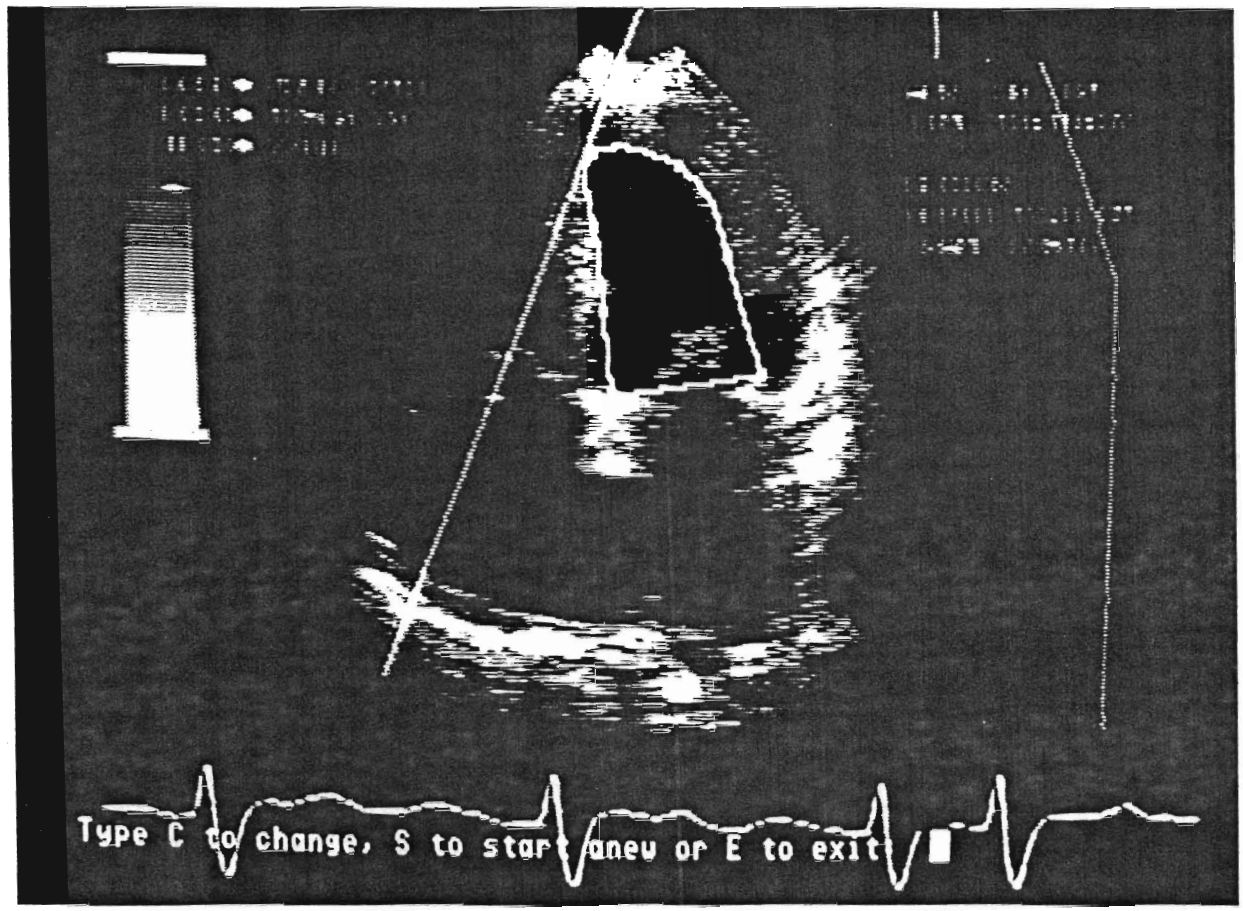

Figure 4d.

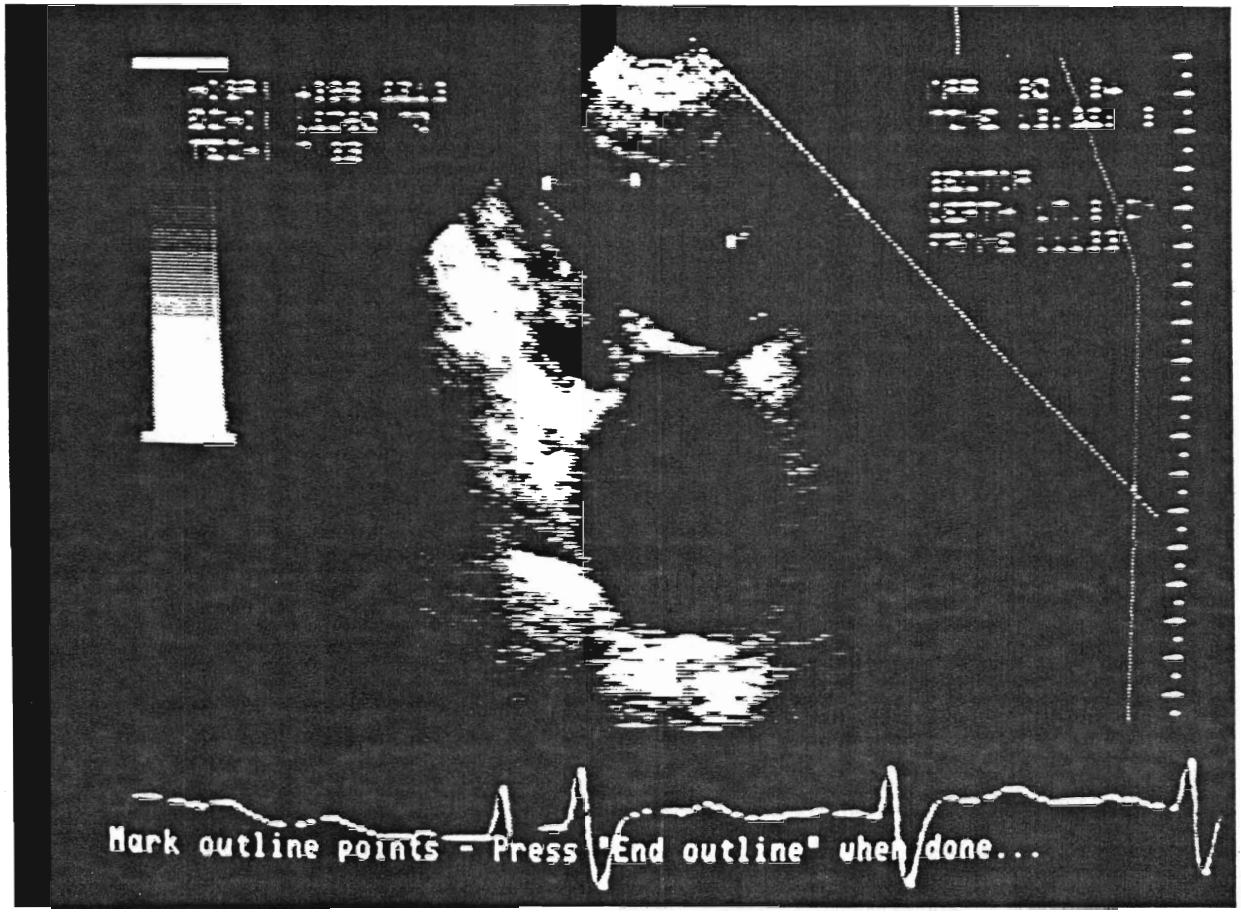

Figure 4e.

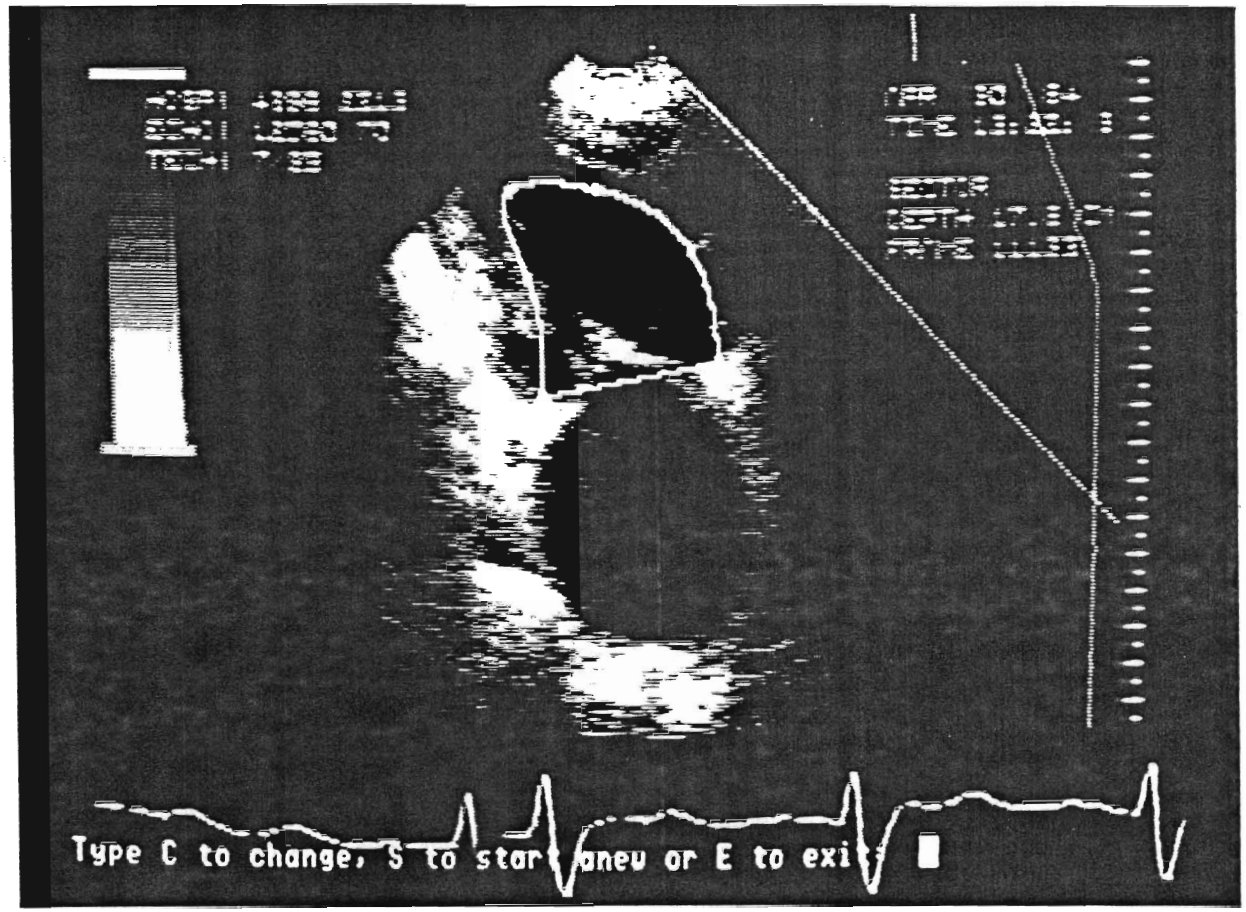

Figure 4f.

therefore not in ascending order with respect to the x-axis. Finally, it must interpolate to an arbitrary number of data points which are arbitrarily spaced and must be free of irregularities and undulations in segments where a large change of slope or curvature occurs from point to point (Figures 4e and 4f). The correctly applied cubic spline can meet these constraints efficiently to produce a curve judged most visually acceptable by medical personnel(11).

The SBD system allows an operator to enter, change or delete data points in random order. The points must therefore be sorted into a circular format, accomplished in the present application by calculating the geometric centroid of all data points, translating them into polar coordinates, and arranging them in ascending order by angle via a simple bubble sort(12). A smooth curve may be generated through the circular configuration using a parameterization of the standard cubic spline which is derived as follows(13):

A new parameter $Z_i(a_i,y_i)$ is defined for $i = 1,\ldots,n$ where, in terms of the previous section, a_i and y_i are the cartesian coordinates of any data point. Z_i is calculated as follows:

$$Z_1 = 0$$

$$Z_i = Z_{i-1} + d_i \text{ for } i = 2,\ldots,n$$

where $Z_n \leq$ curve length and in the present application

$$d_i = \sqrt{(a_i - a_{i-1})^2 + (y_i - y_{i-1})^2}$$

Using this formula Z_i simply becomes the distance in chordal lengths from (a_1,y_1) to (a_i,y_i).

In the production of the smooth curve in Figure 2c, only data points on the x and y plane were involved in the calculation, and only one pass through the spline algorithm was required to generate all S(x) over the interval I. In a parametric spline two sets of transformed data points are generated, $\{Z_i,a_i\}$ and $\{Z_i,y_i\}$. Passing the first set $\{Z_i,a_i\}$ into the standard cubic spline algorithm yields the function $S_a(z) = x$ and passing the second set $\{Z_i,y_i\}$ into same yields the function $S_y(z) = S(x)$, for which of course $Z_1 \leq z \leq Z_n$. Given the appropriate end conditions (to be described presently) plotting the resulting x and S(x) coordinates produces the curves in Figure 4. Note that the only major differences between the standard cubic spline and the parametric spline are:

1. Definition of data points.
2. Number of passes through the algorithm (number of spline functions that must be generated).

Note that in the derivation of the standard cubic spline among the necessary constants to be determined λ_1, d_1, μ_n, and d_n, are undefinable (Eq.9) given the interval I =[a,b], since there is no data point information outside that interval. Therefore, certain end conditions must be incorporated into the spline algorithm in order to determine the behavior of the resulting function at the endpoints of the interval. Several end conditions are possible, the simplest employing the assumption that S"(a) = S"(b) = 0. These end conditions produce the natural cubic spline, which can be seen from Figure 2c to behave linearly near the endpoints. This type of spline has been employed in the present research to produce the curves in Figures 4d and 4f, which are open-ended and are

more naturally linear near the endpoints due to the shape of the left ventricular silhouette in the given cross-sectional views. The natural cubic spline is easily derived from the standard cubic spline algorithm by setting $\lambda_1 = d_1 = \mu_n = M_1 = M_n = 0$ (9). The same end conditions may be applied to a parametric spline, which has been done in the present application.

In Figure 4b, the circular closed curve was actually produced using a natural cubic parametric spline with two minor modifications. The curve was closed by introducing a new data point (a_{n+1},y_{n+1}) where $a_{n+1} = a_1$ and $y_{n+1} = y_1$ and calculating the parametric spline for the new interval $I = [a,b]$ where $a = a_1$ and $b = a_{n+1} = a$. Figures 5a and 5b illustrate the original ordering of n data points and the new ordering of n+1 data points to obtain the closed curve.

In order to avoid irregularities in curvature at the starting/ending point of the curve two additional new data points were created, (a_0,y_0) and (a_{n+2},y_{n+2}), where $a_0 = a_n$, $y_0 = y_n$, $a_{n+2} = a_2$, and $y_{n+2} = y_2$ (Figure 5c)(14). The information at nodes a_0 and a_{n+2} may then be used to determine $S''(a_1)$ and $S''(a_n)$, or M_1 and M_n in the terms of the standard cubic spline derivation (pg. 5). The natural cubic parametric spline is then calculated over the interval $I = [a,b]$ where $a = a_1$ and $b = a_{n+1}$ and the curve shown in Figure 5c results.

Implementation of Border Definition Techniques

Both the manual and semi-automatic contouring systems were developed on the Diasonics Cardio Revue Center, a commercially available computerized echocardiographic quantification system consisting of a Z80A 64k byte microprocessor, 256 x 256 pixel monitor, magnetic bitpad

Figure 5. Ordering of data points and resulting qualitative curves

a. An example of n=7 data points which have been sorted into ascending order by angle with respect to their geometric center of mass (left) and the resulting parametric cubic spline calculated from n=7 data points (right).

b. Ordering of n+1=8 data points which have been sorted into ascending order by angle with respect to the geometric center of mass of the first n data points, where $a_1 = a_{n+1}$ and $y_1 = y_{n+1}$ (left) and the resulting parametric cubic spline calculated for n+1 data points (right).

c. Ordering of n+2 data points which have been sorted into ascending order by angle where $a_0 = a_n$, $y_0 = y_n$, $a_1 = a_{n+1}$, $y_1 = y_{n+1}$, $a_2 = a_{n+2}$, and $y_2 = y_{n+2}$ (left) and the resulting curve calculated for $\{a_i, y_i\}$ for $i = 1,\ldots,n+1$ where M_1 and M_n are determined from the information provided by nodes a_0 and a_{n+2}.

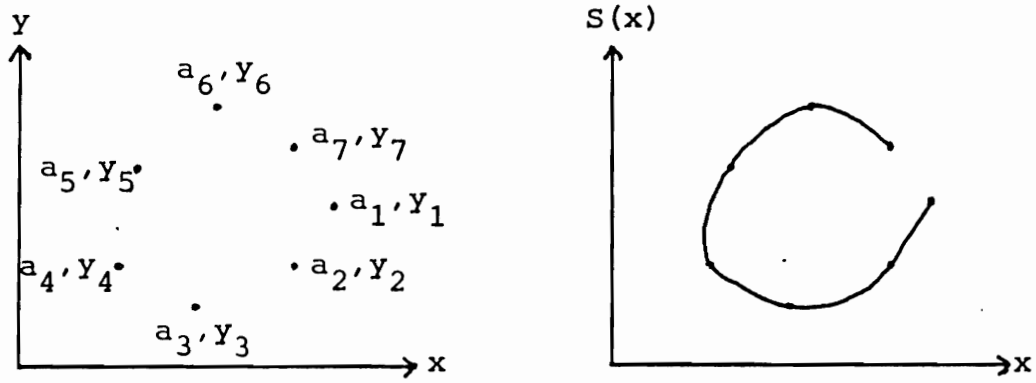

Figure 5a.

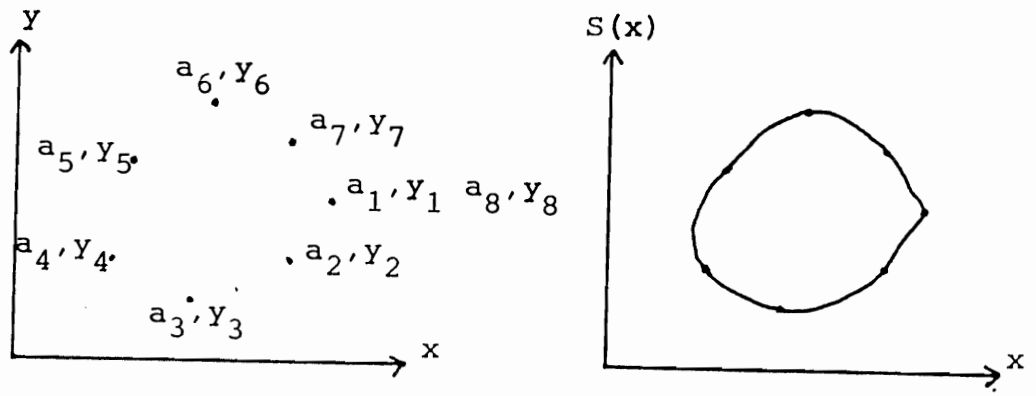

Figure 5b.

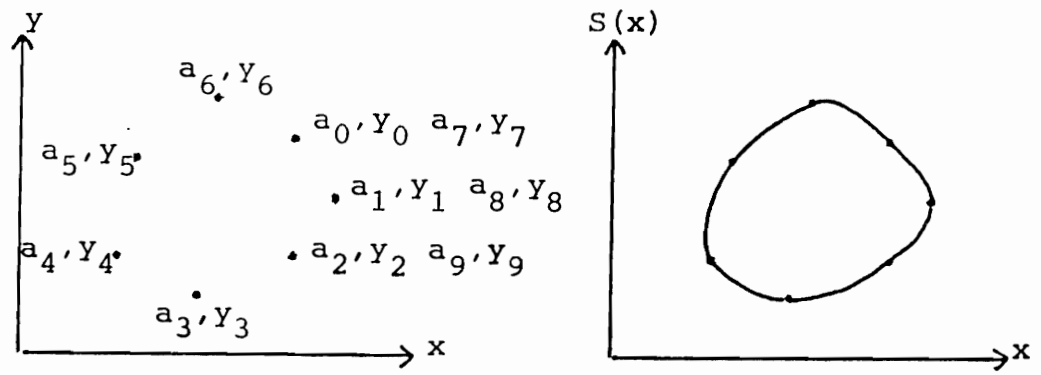

Figure 5c.

and pen, 2 5-1/4 inch floppy disc drives, a 5 megabyte winchester disc drive, an Epson printer, and a 1/2 inch videotape JVC BR - 6400U video-cassette recorder. All clinical software was written in UCSD Pascal.

Diasonics commercial software included a system for MBD and quantification via two-dimensional echocardiograms. This system was modified and incorporated into the present project along with the newly-developed SBD method.

MBD is accomplished by tracing the presumed chamber outline with the pen and bitpad. When the pen touches the bitpad a cursor appears on the monitor and when pressure is applied a line is drawn on the monitor from the most recent previous pressure point to the current point. The coordinates of the current point are added to the contour buffer. If the current point is within a small radius of the previous point, no line is drawn and no coordinates are recorded, thus preventing storage of redundant data. Bitpad coordinates are calibrated to screen coordinates. If the observer wishes to erase he can do so by pressing "erase" in the command section of the bitpad and the points will be erased from the monitor and removed from the contour buffer starting with the most recent point and continuing backward until the pen is removed from the "erase" command. The contour is completed by pressing the "end outline" command.

In the present implementation of SBD the observer enters several RBPs via the pen and bitpad. The experienced observer can exercise informed RBP placement and spacing in order to avoid contour regeneration. The observer may enter points in random order and may erase a point at anytime by pressing the "erase" command and then pressing the

point to be erased. When satisfied with the placement of the RBPs, the observer presses the "end outline" command. The software then utilizes the cubic spline algorithm previously described to generate a smooth parametric curve through all points. If the resulting contour needs correction the observer can add, delete, or change RBPs and the contour will be regenerated.

Production and Selection of Images and Contours

In the present research stop-frame images from real-time two-dimensional echocardiographic clinical studies and computer-generated phantom images were used to compare border definition techniques.

Five fair to very good quality clinical studies were chosen for analysis. All five clinical studies were considered by an experienced echocardiographer to display a mild to severe structural and/or functional abnormality of the left ventricle. These were chosen in order to provide a representative sample of possible left ventricular shapes. Clinical studies were performed by experienced echocardiographic technicians using a Diasonics C-3400R or CV-3400R Phased Array Ultrasonograph using standard echocardiographic imaging techniques as described by Hagan et al.(15). Studies were recorded on half-inch videotape using a JVC BR - 6400U videocassette in order to save operator time.

After transfer, each patient study included only three tomographic cardiac planes: parasternal short axis at the mitral valve level (SAM), apical four-chamber (A4CH), and apical two-chamber (A2CH). These are the cardiac views of interest in the attainment of regional wall motion and thickening indices for which accuracy and reproducibility of radial or segmental area measurements of the left ventricle

are a primary concern. The transducer and plane orientation as well as a stop-frame of the resulting image are demonstrated for SAM in Figure 6, for A4CH in Figure 7, and for A2CH in Figure 8.

For each echocardiographic plane it is possible to generate several contours, each representing a particular chamber, layer of the heart wall, and phase in the cardiac cycle. For the purposes of this study two contours were selected as representative left ventricular outlines for each of the three cardiac planes mentioned above: the endocardial border at end-diastole, where end-diastole was defined by the ECG R-wave, and the endocardial border at end-systole, where end-systole was defined as the point of smallest left ventricular silhouette before mitral valve opening(16). Thus a total of six cardiac contours were generated for each echocardiographic patient study. In order to minimize variability a specific stop-frame was specified for each contour to be generated.

A black-on-white phantom image was generated with the aid of a Siemens Gammasonics Digitron 1 digital image frame buffer and a Sumagraphics magnetic pen and bitpad, interfaced to a Vax 11-750 VMS Computer. This image simulated a probable left-ventricular outline of a parasternal short axis echocardiographic plane (Figure 9). The cartesian coordinates of the phantom image outline were transferred from the Vax to the Cardio Revue Center by hand and were calibrated to correct for the differing aspect ratios of the Digitron and CRC monitors. The phantom image itself was transferred from the Digitron to a 1/2 inch videotape (via the Cardio Revue Center videocassette recorder previously specified), where multiple frames were recorded for

Figure 6. Parasternal short axis echocardiographic plane

a. Stop frame from a real time two-dimensional echocardiogram parasternal short axis view at the mitral valve level at end-diastole, illustrating the right ventricle (RV), septum (S), mitral valve orifice (MVO), and posterior wall of the left ventricle (PW).
b. Transducer and plane orientation used to obtain stop frame in Figure 6a.

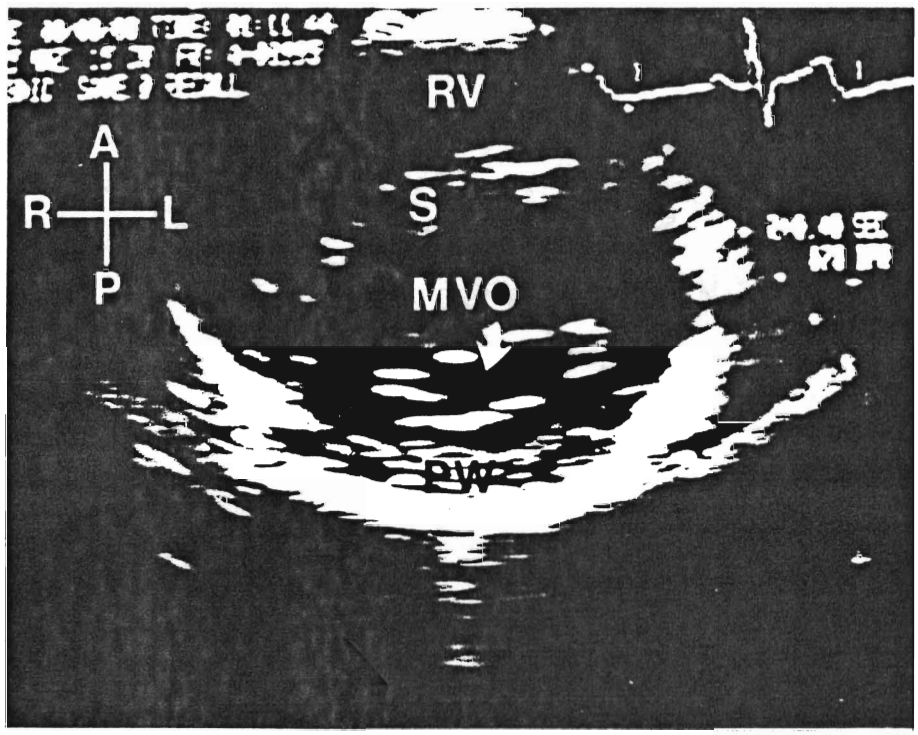

Figure 6a.

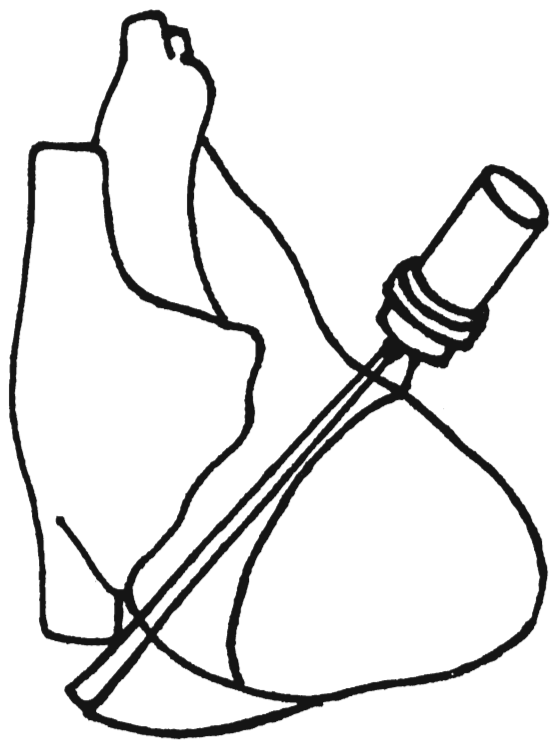

Figure 6b.

Figure 7. Apical four chamber echocardiographic plane

a. Stop frame from a real time two-dimensional echocardiogram apical four-chamber view at end-diastole, illustrating the right ventricle (RV), right atrium (RA), left ventricle (LV), and left atrium (LA).
b. Transducer and plane orientation used to obtain the stop frame in Figure 7a.

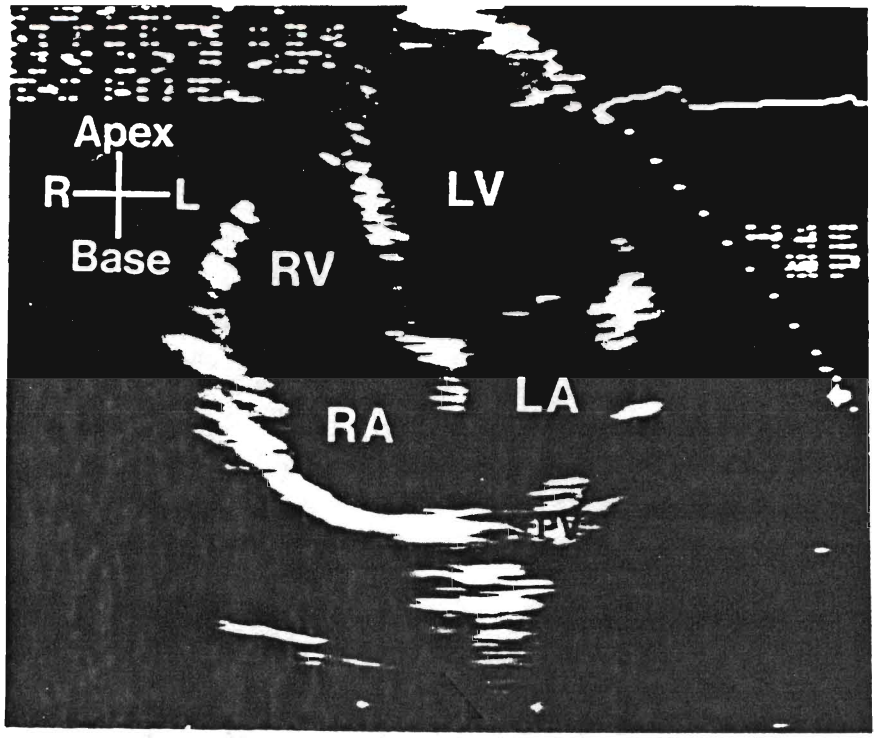

Figure 7a.

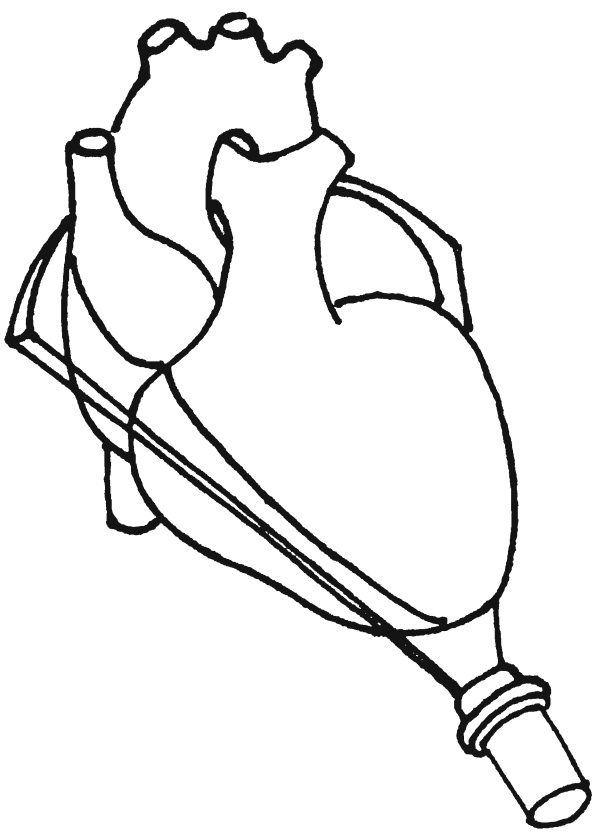

Figure 7b.

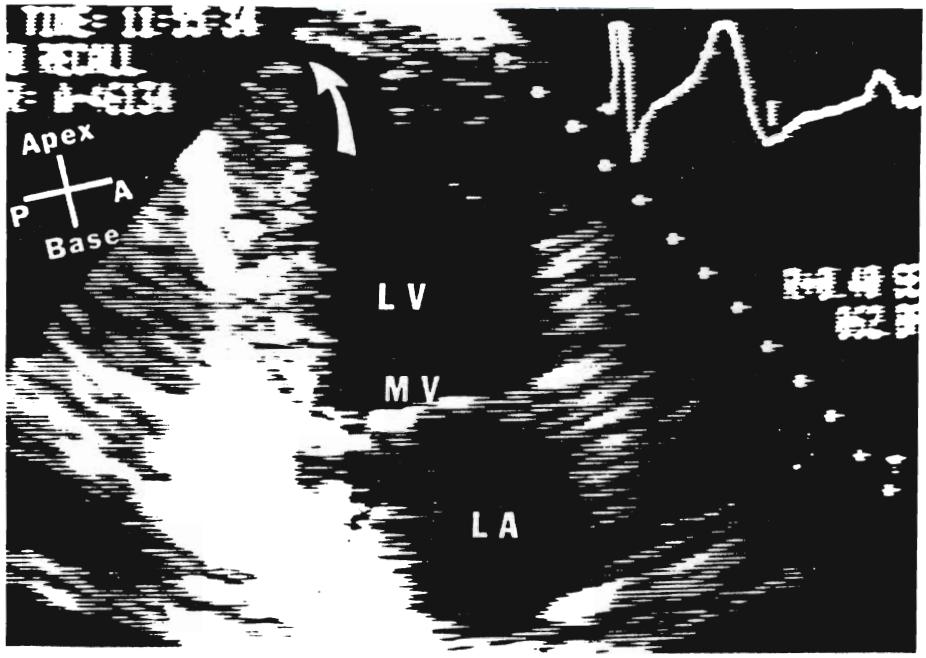

Figure 8a.

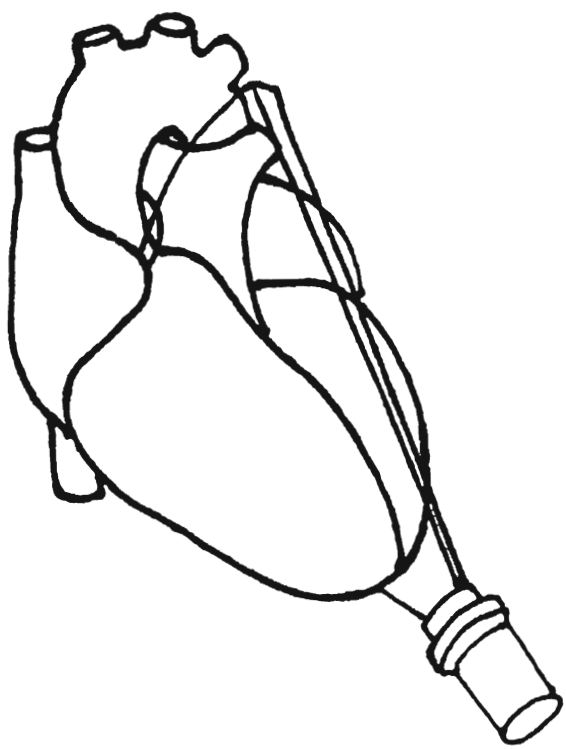

Figure 8b.

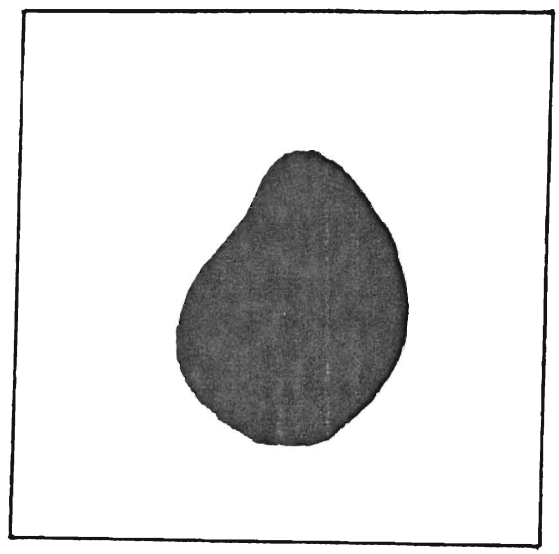

Figure 9. Black-on-white image simulating probable left ventricular outline from the parasternal short axis echocardiographic plane.

Figure 8. Apical two chamber echocardiographic plane

a. Stop frame from a real time two-dimensional echocardiogram apical two-chamber view at end-diastole, illustrating the left ventricle (LV), left atrium (LA), and mitral valve (MV).
b. Transducer and plane orientation used to obtain the stop frame in Figure 8a.

prolonged image visualization without stop-framing.

Quantification of Contours

For contours generated from echocardiographic clinical studies three types of measurements were obtained and recorded for future analysis:

1. Time required for contour generation.
2. Number of RBP's required to generate an acceptable contour as determined by the operator (SBD method only).
3. Sixty-four radial or hemichordal measurements.

The computer system clock was used to time contour generation. In the MBD method this was accomplished by reading the system clock when the operator typed a keystroke to enter the contour generation mode. The clock was read again when the operator signaled completion of the contour by pressing the "end outline" bitpad command. The difference between the two times was recorded in units of seconds.

In the SBD method the system clock was read upon the operator's keystroke to enter contour generation mode, but not again when the operator pressed "end outline," since in the SBD method this command signals the completion of RBP entry rather than of contour generation. Instead, the second reading of the system clock for the SBD method occurred when the operator signaled through a keystroke that the computer-generated contour was acceptable. Alternative keystrokes enabled the operator to make changes or start the contour over in which cases the timing continued without interruption until an acceptable contour was generated. The difference between the two times was recorded in units of seconds, as for the MBD method.

For short axis views the center of mass was calculated by summing the coordinate values for each contour and dividing each sum by the total number of coordinate pairs. Radial measurements were then made from the centroid at 64 angles equally spaced over 360 degrees (Figure 10). The measurements were recorded in units of pixels and no correction was made for aspect ratio.

For apical views the operator was asked to define apex and midbase markers (Figure 11a). An axis was then constructed between the two markers and the point distinguishing the apical from the middle thirds was located (Figure 11b). At this point a second axis was constructed perpendicular to the first and the midpoint of the chord formed by the intersection of this axis with the contour was located (Figure 11c). A third axis was constructed from the midbase marker to the midpoint and all other axes were discarded (Figure 11d). Twenty one points were then defined on the axis which equally subdivided its total length. Hemichordal measurements were obtained by constructing a ray starting from each point of the subdivided axis perpendicular to that axis and determining the length of the hemichord formed by the intersection of the ray with the contour. This calculation was performed on both sides of the axis. The remaining third of the 64 measurements were made radially from the midpoint to the apical outline at equally spaced angles over 180 degrees. Figure 11e demonstrates the configuration of all 64 linear measurements for apical views(16). Measurements from apical views were recorded in ascending circular order starting at the lower left and ending at the lower right.

Only one type of measurement was recorded for contours generated

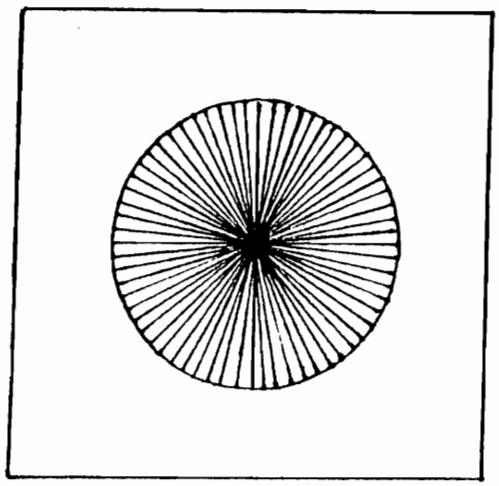

Figure 10. Radial measurements representing the distance from the geometric center of mass to the chamber border at 64 equidistant angles were used to quantify parasternal short axis contours.

Figure 11. Hemichordal measurement of an apical view.

a. Left ventricular outline from an apical view with apex and midbase markers.
b. Axis between apex and midbase with point separating the apical from the middle third.
c. A second axis constructed perpendicular to the first with midpoint of chord formed by intersection with the contour.
d. Third axis constructed from midbase to midpoint.
e. Sixty four hemichordal measurements.

Figure 11.a.

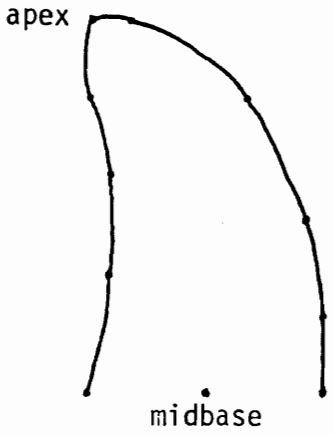

Figure 11.b.

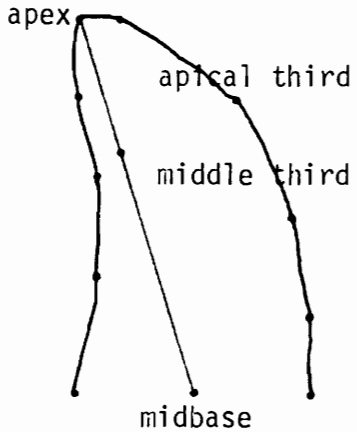

Figure 11.c.

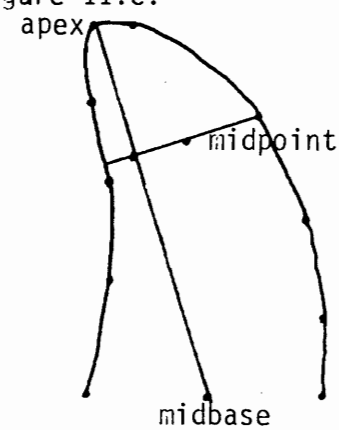

Figure 11.d.

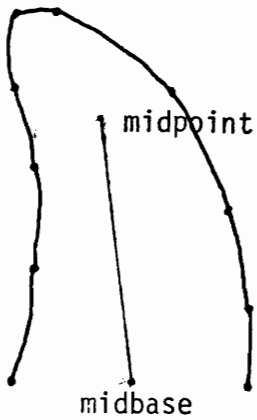

Figure 11.e.

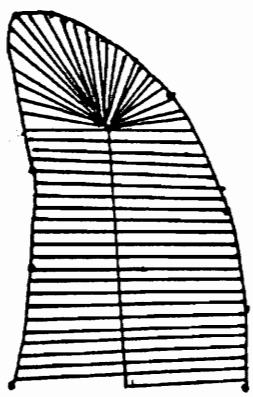

from phantom images. This measurement is best described as a radial difference taken between the true border and the computer generated contour. Sixty four radial differences were calculated for each contour as described below.

Since the true border coordinates of the phantom image outline were known, the true radial lengths were calculated for this outline in the manner previously described for the short axis echocardiographic views (pg.38). When the operator generated a contour representing the phantom outline using either border definition technique, the 64 radial lengths were calculated using the centroid of the true border. The 64 measurements to be used in the analysis were then the absolute radial differences at each angle between the true radial lengths and the operator-defined radial lengths (Figure 12).

Three experienced observers generated all 6 cardiac contours for each of the selected patient studies over several trials. Both the MBD and the SBD methods were applied to each cardiac contour in random order, producing a total of 12 contours per patient study per trial. Left ventricular endocardial borders were identified using the leading edge-to-leading edge techniques described by Wyatt et al.(17). Papillary muscles were included within the confines of the left ventricular borders(16). Darkening of the room and real-time and slow-motion playback were used for better visualization of two-dimensional echocardiographic images. Two observers completed five trials within a period of one to two months and one observer completed three trials in a period of two months.

Seven observers generated contours from the phantom image using both border definition methods over ten trials. For each trial both

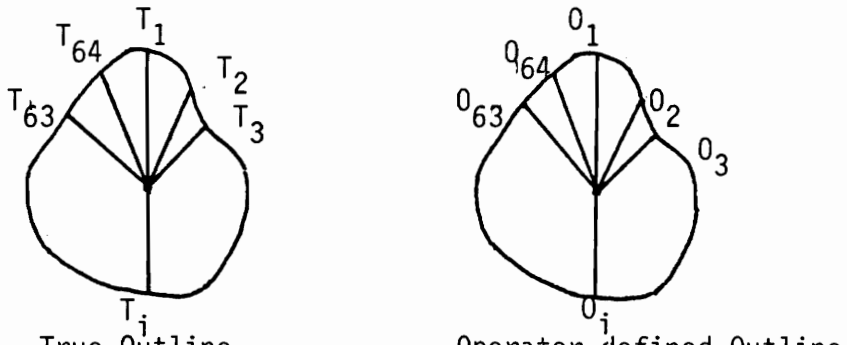

True Outline

Operator-defined Outline

for i = 1,...,64

Absolute Radial Difference = $/O_i - T_i/$

Figure 12. Sixty-four absolute radial differences calculated for contours generated from the phantom image. This was accomplished by taking the difference between the true radial length and the radial length calculated from the operator-defined contour at each of 64 equidistant angles.

border definition methods were applied in random order. Observers had varying levels of experience. Each observer was given approximately one half hour to practice before any data was recorded and all ten trials were generally performed in one sitting.

Analysis of Data

Data from all studies was hand-entered into the Tandem computer where analysis programs were executed in Fortran. All clinical data for each of the 6 cardiac contours were analyzed separately.

Contour generation times from clinical studies were categorized into cells by observer, patient, trial, cardiac contour, and border definition method. Figures 13, 14, and 15 show frequency histograms of contour generation times from each of the 6 cardiac contours studied. Abnormally large time values (over 500 seconds) were considered the result of operator distraction and were eliminated from the analysis in order to prevent skewing of the data. A paired t-test was performed between methods over all cells.

Mean number of RBP's was determined over all patients, trials, and observers for each of the 6 cardiac contours.

In order to compare reproducibility of border definition methods radial or hemichordal length data from each cardiac contour was separated into cells by patient, observer, angle, and method. Two thirds of the data cells contained five trials and one third contained three trials. The variance of each cell was calculated and the cells were paired by border definition method so that a paired sign test (Figure 16), for which the variances served as the paired variates, could be performed(18). Grossly abnormal values, associated with computer

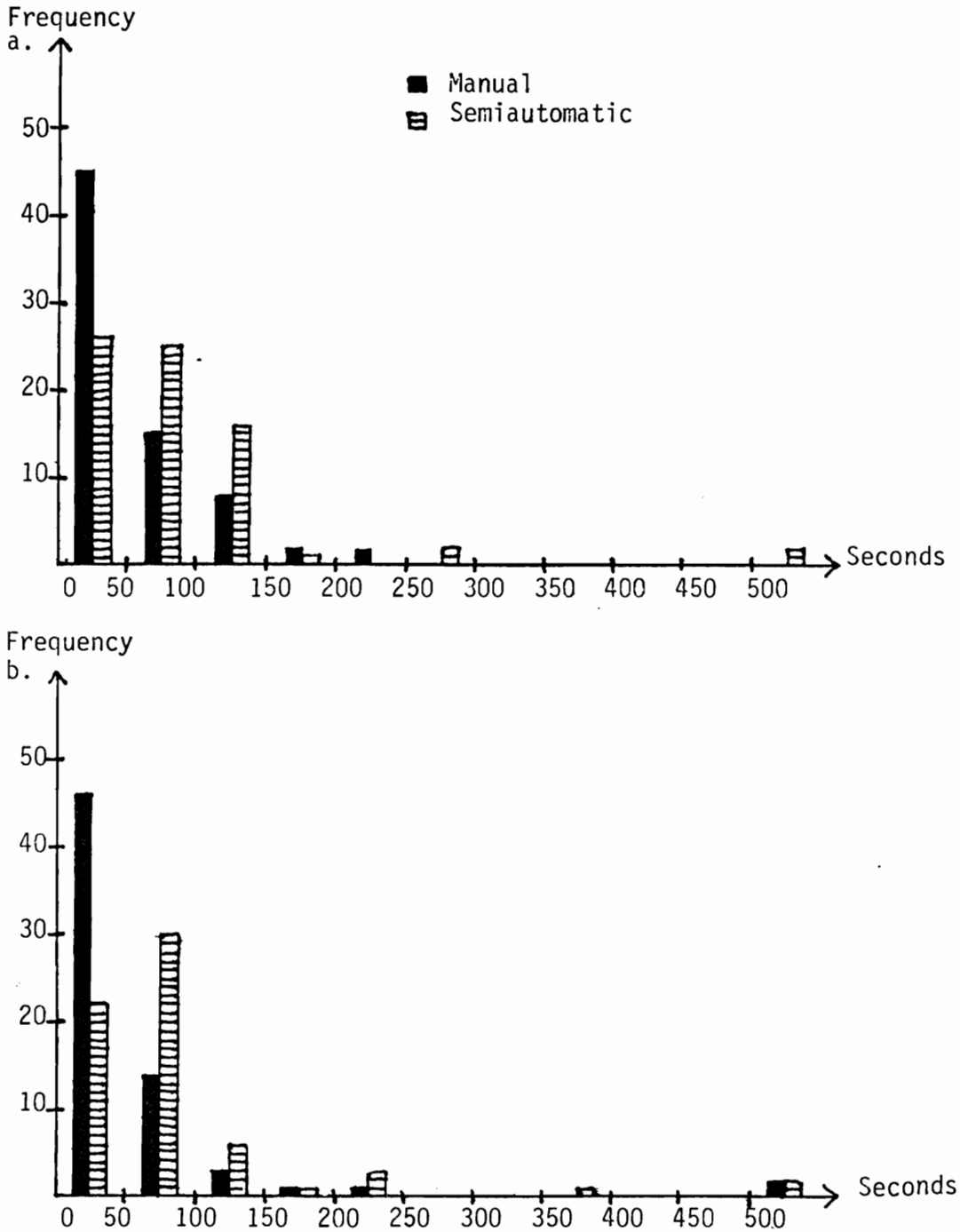

Figure 13. Contour generation times for short axis view

a. Contour generation times for the parasternal short axis view at the mitral valve level at end-systole.
b. Contour generation times for the parasternal short axis view at the mitral valve level at end-diastole.

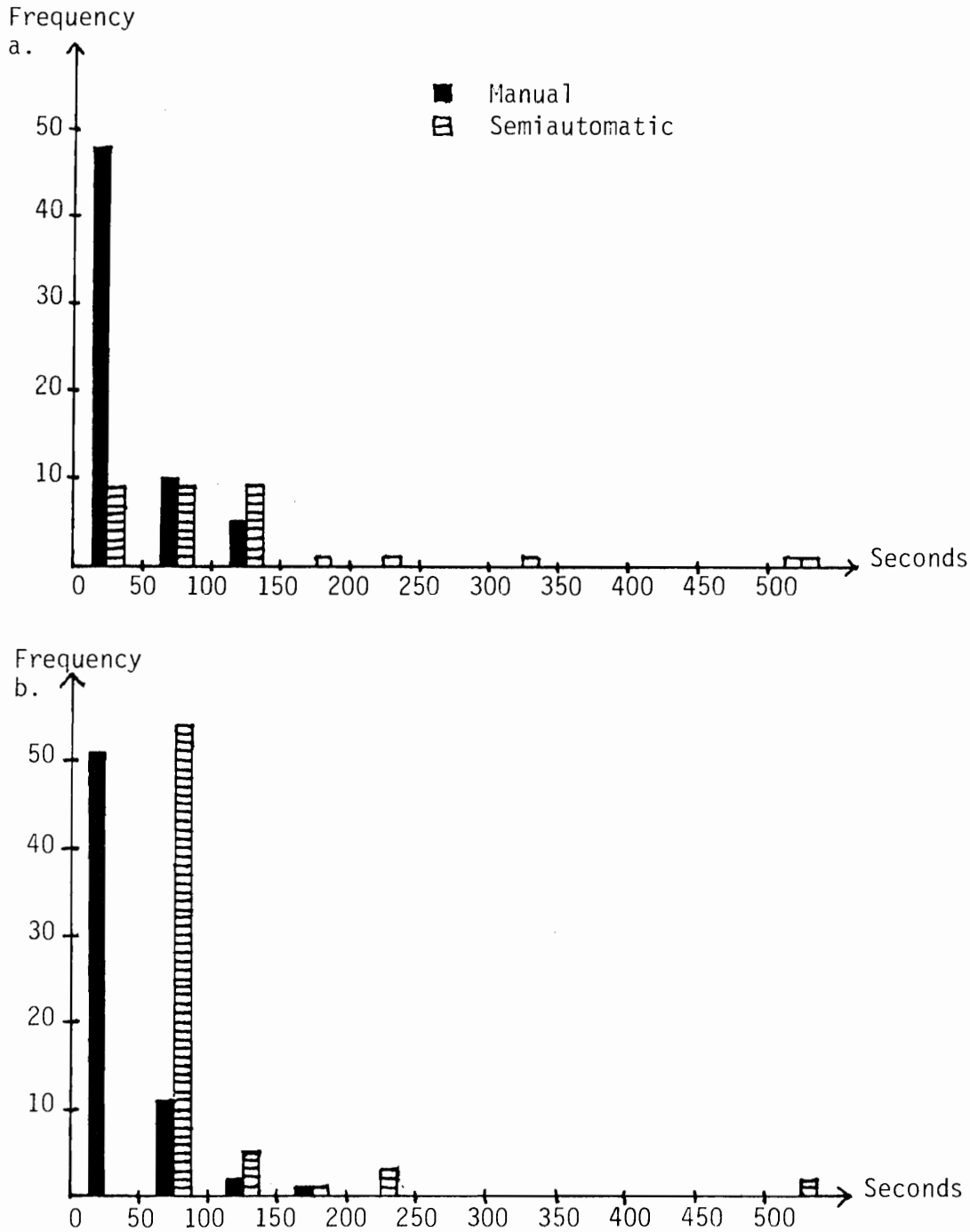

Figure 14. Contour generation times for apical four-chamber view

a. Contour generation times for the apical four-chamber view at end-systole.
b. Contour generation times for the apical four-chamber view at end-diastole.

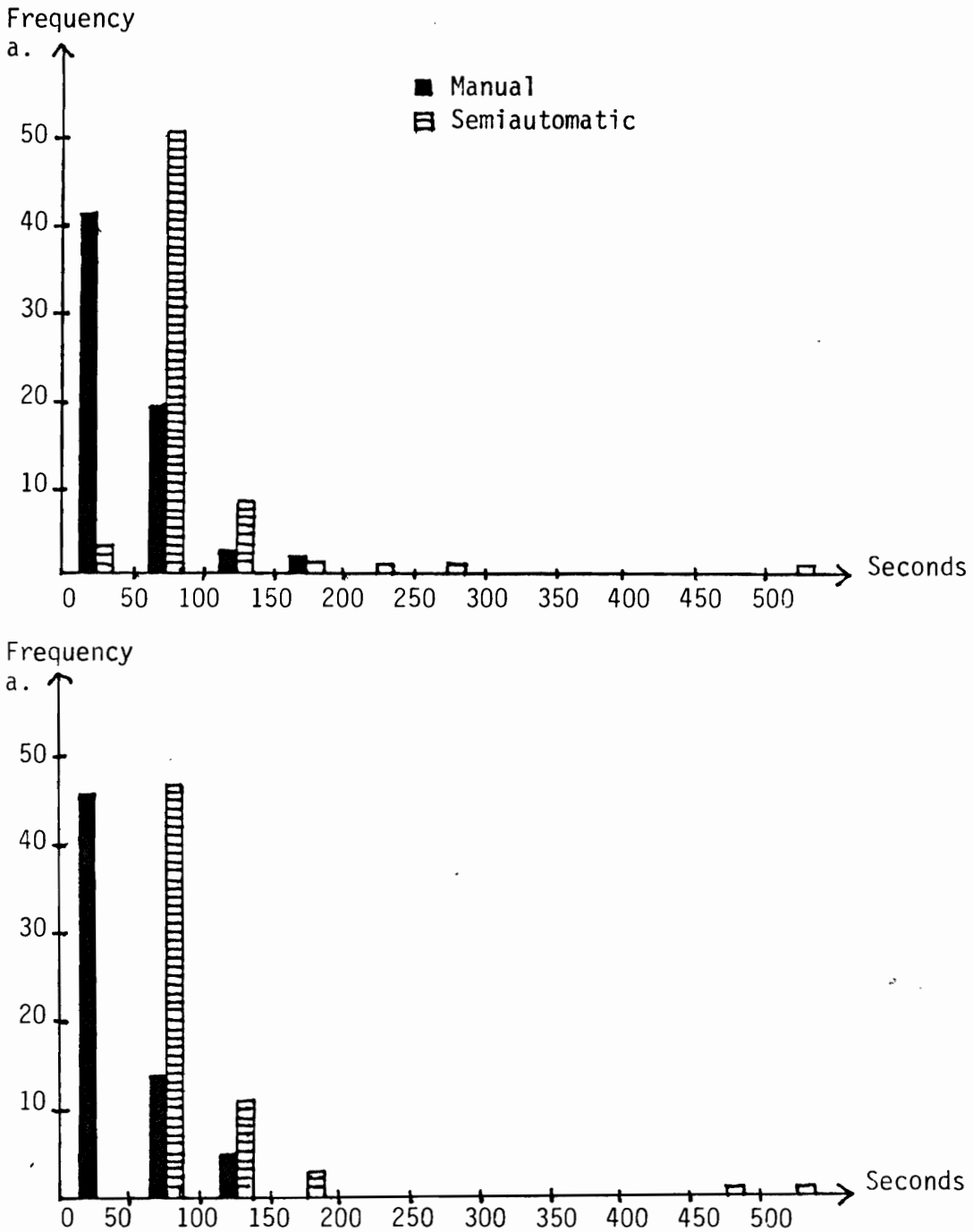

Figure 15. Contour generation times for apical two-chamber view.

a. Contour generation times for apical two-chamber view at end-systole.
b. Contour generation times for apical two-chamber view at end-diastole.

SIGN TEST

Group 1		Group 2		Difference (d)
x_1	-	x_1	=	d_1
.		.		.
.		.		.
.		.		.
x_m		x_m		d_m

* i values of d are less than 0

* n - i values of d are greater than 0

* values of d equal to 0 are ignored

* n = total number of values not equal to 0

THEN:

$$z = \frac{i - \frac{n}{2}}{\sqrt{\frac{n}{4}}}$$

WHERE: $z \sim N(0,1)$

Figure 16. Nonparametric test to determine whether there is a significant difference between two means in a paired experiment.

error in trapping contour coordinates, were eliminated from the analysis.

In the analysis of the phantom data a value representative of the accuracy of the entire observer-defined contour with respect to the true outline was determined by averaging the absolute values of all 64 radial differences associated with a given contour. The resulting mean absolute radial differences were paired by border definition method over all observers and over all trials and analyzed via a standard paired t-test. T-statistics were also determined for the first five trials and second five trials separately in order to determine whether there existed a learning curve that could affect the distribution.

III.

RESULTS

Time Requirements

The mean contour generation time for all six cardiac contours was shown by the paired t-test to be significantly greater for the SBD method. The validity of this result is questionable, since the frequency histograms in Figures 13, 14, and 15 show that the distribution of times is not normal for either border definition method. The histograms do, however, indicate that the MBD distributions peak closer to zero seconds than do the SBD distributions. The median value over all contours for the MBD method was 27 seconds with a low of 7 seconds and a high of 245 seconds, while the median for the SBD method was 67 seconds with a low of 30 seconds and a high of 492 seconds. Median, low and high values for each of the six cardiac contours are outlined in Table 1.

Storage Requirements

No SBD contour required less than 6 or more than 22 RBPs. The mean number of RBPs required to generate an acceptable border over all cardiac contours was 9 with a standard deviation of $\pm$ 3.8. The mean number of RBPs calculated for each cardiac contour along with the associated standard deviations can be seen in Table 2.

TABLE 1

Contour Generation Times for Manual and Semiautomatic Border Definition Methods

Times in units of seconds

cardiac contour	MBD median	MBD low	MBD high	SBD median	SBD low	SBD high
SAM end-systole	31	8	225	54	30	269
SAM end-diastole	32	10	245	59	41	382
A4CH end-systole	21	7	197	67	40	348
A4CH end-diastole	24	9	157	71	52	232
A2CH end-systole	24	8	199	72	47	260
A2CH end-diastole	26	8	141	78	54	492

TABLE 2

Mean Number of Representative Border Points Used for Contour Generation by the Semiautomatic Border Definition Method

cardiac contour	mean number of representative border points	sd
SAM end-systole	7.52	2.58
SAM end-diastole	8.05	4.27
A4CH end-systole	8.86	2.68
A4CH end-diastole	9.35	2.84
A2CH end-systole	9.78	6.22
A2CH end-diastole	10.37	6.22

Reproducibility

Reproducibility of the MBD and SBD methods was compared via a sign test of radial or hemichordal measurements as previously described. The sign test results are outlined in Table 3. It can be seen that the SBD method produced left ventricular contours that were significantly more reproducible in both of the SAM contours and in the A4CH view at end-systole and A2CH at end-diastole. Of the remaining apical contours two, A4CH at end-systole and A2CH at end-diastole, showed no significant difference in reproducibility between methods. Only one out of the six cardiac contours, A2CH at end-diastole, proved to be significantly more reproducible when generated by MBD.

Table 4 shows the mean variance for each contour and border definition method in units of pixels squared. It is important to note that the mean variance of radial measurements from the A4CH at end-diastole was significantly larger for the SBD method than for the MBD method. This apparent contradiction to the results of the sign test is explained by the nonparametric nature of the measurements. A few aberrantly large variances, possibly undetected computer errors, will significantly skew the mean, but this phenomenon does not affect the outcome of the sign test.

Accuracy

The results of the paired t-test on phantom data are shown in Table 5. It can be seen that all three combinations of trials showed the mean 'mean absolute radial difference' to be significantly less for the SBD technique. A more significant difference was indicated during the second half of the learning curve over the ten trials than during the first half.

TABLE 3

Sign Test Analysis Comparing Variances of Radial or Hemichordal Lengths Between Manual and Semiautomatic Border Definition Methods

cardiac contour	i*	n-i*	n	z	p
SAM end-systole	281	675	956	-12.74	.000
SAM end-diastole	231	701	932	-15.39	.000
A4CH end-systole	497	451	948	1.49	.136
A4CH end-diastole	409	546	955	-4.43	.000
A2CH end-systole	464	405	869	2.00	.046
A2CH end-diastole	437	447	884	-.336	.784

* i = number of cells for which the MBD variance was less than the SBD variance

* n-i = number of cells for which the MBD variance was greater than the SBD variance

TABLE 4

Mean Variances of Radial or Hemichordal Measurements for Manual and Semiautomatic Border Definition Methods

cardiac contour	MBD(pixels)^2	SBD(pixels)^2
SAM end-systole	2.149	1.907
SAM end-diastole	4.518	1.229
A4CH end-systole	1.730	1.815
A4CH end-diastole	1.736	4.127
A2CH end-systole	6.317	4.127
A2CH end-diastole	4.426	4.824

TABLE 5

Results of Paired T-Test Comparing Mean Absolute Radial Differences Between Manual and Semiautomatic Border Definition Methods

Trials	t	df	p
1 - 5	4.68	34	.000
6 - 10	5.77	34	.000
1 - 10	7.39	69	.000

IV.

DISCUSSION

Several factors are involved in the production of accurate and reproducible quantitative measurements from two-dimensional echocardiographic images. These include echocardiographic technique, image quality, border identification technique, time constraints, quantification method, experience level of operators, and border definition method.

In the present research, echocardiographic technique and experience level of operators are assumed to be optimal.

Image quality of the patient studies used in this research was moderate to very good. However, images may have been slightly degraded by transfer to a second videotape and by repeated and prolonged freezing of the frames selected for contour generation. An attempt was made to include images and cardiac views of the quality and type that would be most likely candidates for quantification, especially of regional wall motion and thickening indices.

It is projected that images of improved quality may ameliorate the reproducibility of SBD contours more than that of MBD contours. This theory is evidenced by the results of the phantom study which indicate that when border identification error is eliminated, SBD produces a more accurate border than does MBD. Additionally, the inherent discrepancy

in border visualization between short axis and apical views may explain the comparatively average performance of SBD in three out of the four apical contours. Short axis views are in general more easily visualized than apical views and are subject to less echo dropout. Apical views are frequently clouded or even clipped at the apex and the endocardium is poorly visualized or unidentifiable along the lateral wall of the left ventricle.

Image quality is affected by a number of variables. Among these are type and configuration of transducer, dynamic range of the system, levels of time variable gain, depth of penetration, line density of the sector, frame rate of the recording system, pulse repetition rate, quality and condition of the videotape, and echocardiographic technique. Most of these factors are not under the control of echocardiographers or echocardiographic technicians, but improvement of image quality is a continuing effort among designers of ultrasonic instruments. At present, however, further studies comparing the reproducibility of the SBD and MBD methods using optimum quality images are needed in order to substantiate the theory that the superiority of SBD is ameliorated with improved image quality.

Other factors associated with the difference in comparative reproducibility between short axis and apical contours may be related to the shapes of the left ventricular outlines. Subjectively, observers found it to be a more natural motion to draw the open-ended banana shape of the apical views than to draw the closed circular shape of the short axis views. Alternatively, the spline algorithm is naturally suited to circular shapes and requires a minimum number of RBPs to produce an

acceptable contour. Apical views require more RBPs for contour generation and this factor combined with the increased ambiguity of border visualization in these views may result in greater potential error in the SBD method.

Border identification is one of the most significant difficulties in the generation of accurate and reproducible two-dimensional echocardiographic contours. Studies have shown that the leading edge-to-leading edge technique used in the present research produces the most accurate linear and cross-sectional measurements of myocardial thickness(17). However, for adequate border visualization real-time and slow-motion playback must be carefully applied to each segment of the projected border, and special attention directed toward distinguishing the papillary muscles from the actual myocardium. This process is slow and tedious regardless of border definition method employed. Thus the accuracy and reproducibility of contours is greatly affected by the time constraints and self-discipline of the operator of the echocardiographic quantification system. There is little motivation for most observers to seek maximum accuracy in border definition since there is no means by which accuracy of resulting contours can be evaluated. Thus time requirements and ease of use become key factors in the generation of accurate and reproducible contours.

SBD was considered to be much less tedious than MBD by participants in the present research. Comparison of time requirements between methods showed SBD to be significantly more time consuming than MBD. However, contour generation time using SBD is highly machine-dependent,

since the spline algorithm requires multiple real number calculations for which speed of completion is directly related to microprocessor capacity. Spline calculation on the Cardio Revue Center requires 35-45 seconds, depending upon the number of RBPs utilized, for each contour generation. Thus anywhere from 30% to 90% of each SBD contour generation time from the present data can be considered operator-waiting time. SBD contour generation times may be further increased by operator distraction during the waiting period when the operator's attention is not directly required by the computer.

Spline calculation time could be potentially reduced to zero through implementation of SBD on a system with a high-capacity 16-bit microprocessor (i.e. MC68000). Implementation of the spline algorithm in machine code or assembly language could also reduce time requirements. This improvement would enable SBD contour generation times to rival those of the MBD method. Further studies on a high capacity microprocessor-based system are needed to substantiate this theory.

Accuracy and reproducibility of contours is somewhat dependent upon quantification method. Regional left ventricular wall motion is evaluated through calculation of percent segmental area shrinkage or percent radial or hemichordal shortening from end-diastole to end-systole. Studies have shown that the area shrinkage method is more reproducible and demonstrates more predictive accuracy in the identification of regional wall abnormalities and possible infarct sites(3,19). A satisfactory algorithm for quantitation of regional left ventricular wall thickening via segmental areas has not yet been presented. Wall thickening can, however, be quantified via linear measurements as

described by Moreno et al.(16). Since radial or hemichordal measurements do provide clinically meaningful indices of left ventricular wall motion and thickening(16) and since they are much better suited to the limited real number capacity of the available microprocessor, these measurements were considered the most suitable means of quantifying contour accuracy and reproducibility in the present research.

Linear measurement calculation for both border definition methods was affected by aspect ratio. Since measurements were determined in pixels with no attempt to correct for the monitor's approximate 3/4 (horizontal/vertical) aspect ratio, measurements taken at angles nearly vertical were magnified compared to measurements taken at angles more nearly horizontal. This aberration in measurement was not relevant to the analysis of the clinical studies, since the sign test used to compare variances between methods only compared cells described by the same angle. In the phantom studies the affect of the aspect ratio may have been more pertinent, since a single value was generated to represent all 64 radial measurements from each contour. Consequently, drawing errors at various angles were weighted differently in terms of severity. Since a large sample size was used it is projected that angular weighting of measurements was random enough to have little effect on the outcome of the phantom study.

A hardware limitation in the accurate calculation of linear measurements using the Cardio Revue Center was the resolution of the monitor. The present display screen consists of a 256 x 256 pixel grid which offers limited resolution of real number measurements. A 512 x 512 pixel grid would present a visually more acceptable contour and would

allow more precise calculation of radial measurements.

A final topic of discussion involves the number of RBPs necessary to generate an acceptable contour as determined by the observer. Number of RBPs appears to be highly observer-dependent. In the present research observers were not instructed to use a minimum number of border points, since increased attention to this aspect of semiautomatic contouring tends to increase contour generation time. Of the three observers who generated contours from the five clinical studies, observer 1 had a low RBP number of 6 and a high of 12, observer 2 had a low of 6 and a high of 15, and observer 3 had a low of 8 and a high of 22. A projected theory is that informed placement of the minimum required number of RBPs minimizes error by minimizing subjective judgements made by observers. Again, more studies are needed to compare reproducibility of contours where RBP number is the only variable in order to lend evidence concerning this theory.

V.

CONCLUSIONS

The semiautomatic two-dimensional echocardiographic contouring system appears to have the following advantages over the manual contouring system presently in clinical use:

1. Short axis contours generated using SBD are significantly more reproducible and the majority of apical contours appear equally as reproducible as those generated via MBD.
2. SBD contours require an experimental mean of 9 and a maximum of 22 cartesian coordinate pairs for contour storage with maximum preservation of integrity while MBD contours require 64 or more coordinate pairs.
3. SBD has the potential to be as timely as MBD or even more timely.
4. SBD contours are more accurate than MBD contours when the border is well defined.
5. SBD appears to be less tedious and less fatiguing for the operator than MBD.

Because of these advantages and because it has an even greater potential in the future as hardware modifications are implemented and image quality is improved, SBD appears to be a viable alternative to MBD for two-dimensional echocardiogram contour generation at the present time. Future developments in automated border definition may eliminate

the necessity for manual or semiautomatic methods and it is a likely possibility that spline interpolation could be used in conjunction with automated point recognition techniques to produce the least subjective and most accurate contour of any of the current methods. Thus the algorithm designed for this study has significant potential in the realm of two-dimensional echocardiographic border definition.

REFERENCES

1. Weiss JL, Bulkley BH, Hutchins GM, Mason SJ: Two-dimensional Echocardiographic Recognition of Myocardial Injury in Man: Comparison with Postmortem Studies. Circulation, 63(2):401, 1981

2. Moynihan PF, Parisi AF, Folland ED, Jones DR, Jeldman CL: A system for quantitative evaluation of left ventricular function with two-dimensional ultrasonography. Medical Instrumentation, 14(2):111, 1980

3. Parisi AF, Moynihan PF, Folland ED, Feldman CL: Quantitative Detection of Regional Left Ventricular Contraction Abnormalities by Two-dimensional Echocardiography. II. Accuracy in Coronary Artery Disease. Circulation, 63(4):761, 1981

4. Skorton DJ, McNary CA, Child JS, Newton FC, Shah PM: Digital Image Processing of Two-Dimensional Echocardiograms: Identification of the Endocardium. Am. J. Cardiology, 48:479, 1981

5. Garcia E, Ezekiel A, Levy R, Zwehl W, Ong K, Corday E, Areida J, Meerbaum S, Corday S: Automated Computer Enhancement and Analysis of Left Ventricular Two-Dimensional Echocardiograms. Computers in Cardiology, p784, 1982

6. Garcia E, Gueret P, Bennett M, Corday E, Zwehl W, Meerbaum S, Corday S, Swan HJC, Berman D: Real time computerization of two-dimensional echocardiography. Am. Heart J., 101(6): p.783, 1981

7. Heng MK, Wyatt HL, Meerbaum S, Woythaler J, Hestenes J, Davidson, R, Corday E: An Analysis of the Reproducibility of 2-Dimensional Echocardiographic Measurements. AM. J. Cardology, 41:390 (abstract), 1978

8. Martin RP, Rakowski H, Kleiman JH, Beaver W, London E, Popp RL: Reliability and Reproducibility of Two Dimensional Echocardiographic Measurement of the Stenotic Mitral Valve Orifice Area. Am. J. Cardiology, 43:560, 1979

9. Ralston A, Rabinowitz R: A First Course in Numerical Analysis. New York, San Francisco, McGraw Hill Book Company, p 73, 19

10. Dahlquist G, Bjorck A: Numerical Methods. Englewood Cliffs, New Jersey, Prentice-Hall, Inc., p 132, 166, 1984

11. Garrison JB, Weiss JL, Maughan WL, Tuck OM, Guier WH, Fortuin, NJ: Quantifying Regional Wall Motion and Thickening in Two-Dimensional Echocardiography with a Computer-aided Contouring System. Computers in Cardiology, p 25, 1977

12. Glinert E: Introduction to Computer Science Using Pascal. Englewood Cliffs, New Jersey, Prentice-Hall, Inc. p 327, 1983

13. Dierckx P: Algorithms for Smoothing Data with Periodic and Parametric Splines. Computer Graphics and Image Processing, 20(3):283, 1982

14. Harada K, Nakamae E: An Isotropic Four-Point Interpolation Based on Cubic Splines. Computer Graphics and Image Processing, 20(3):283, 1982

15. Hagan AD, DiSessa TG, Bloor CM, Calleja HB: Two-dimensional echocardiography. Clinical-pathological correlations in adult and congenital heart disease. Boston, Toronto, Little-Brown and Company, pl, 1983

16. Moreno FL, Hagan AD, Gaubert AF, Pryor TA, Hagan LM, Holmen JR: The Clinical Role of Computerized Quantitative Analysis of Regional Wall Function by Two-dimensional Echocardiography. Unpublished, Cardiology Division and Department of Medical Biophysics and computing, LDS Hospital and University of Utah School of Medicine, SLC, Ut 1983

17. Wyatt HL, Haendchen RV, Meerbaum S, Corday E: Assessment of Quantitative Methods for 2-Dimensional Echocardiography. Am J. Cardiology, 52:396, 1983

18. Alder HL, Roessler EB: Introduction to Probability and Statistics, 4th ed. San Francisco, London, W.H. Freeman and Company, p 164, 1968

19. Moynihan PF, Parisi AF, Feldman CL: Quantitative Detection of Regional Left Ventricular Contraction Abnormalities by Two-dimensional Echocardiography. I. Analysis of Methods. Circulation, 63(4):752, 1981